ATOMIZATION, DROP SIZE, AND PENETRATION FOR CROSS-STREAM WATER INJECTION AT HIGH-ALTITUDE REENTRY CONDITIONS WITH APPLICATION TO THE RAM C-I AND C-III FLIGHTS

by Paul B. Gooderum and Dennis M. Bushnell

Langley Research Center
Hampton, Va. 23365

NATIONAL AERONAUTICS AND SPACE ADMINISTRATION • WASHINGTON, D. C. • JULY 1972

1. Report No.	2. Government Accession No.	3. Recipient's Catalog No.
NASA TN D-6747		

4. Title and Subtitle	5. Report Date
ATOMIZATION, DROP SIZE, AND PENETRATION FOR CROSS-STREAM WATER INJECTION AT HIGH-ALTITUDE REENTRY CONDITIONS WITH APPLICATION TO THE RAM C-I AND C-III FLIGHTS	July 1972
	6. Performing Organization Code
7. Author(s)	8. Performing Organization Report No.
Paul B. Gooderum and Dennis M. Bushnell	L-8004
	10. Work Unit No.
9. Performing Organization Name and Address	117-07-04-08
NASA Langley Research Center Hampton, Va. 23365	11. Contract or Grant No.
	13. Type of Report and Period Covered
12. Sponsoring Agency Name and Address	Technical Note
National Aeronautics and Space Administration Washington, D.C. 20546	14. Sponsoring Agency Code

15. Supplementary Notes

16. Abstract

Atomization, drop-size, and penetration data are presented for cross-stream water injection at conditions simulating high-altitude reentry (low Weber number, high static temperature, high Knudsen number, and low static pressure). These results are applied to the RAM C-I and C-III flights. Two primary breakup modes are considered, "vapor pressure" or "flashing" and aerodynamic atomization. Results are given for breakup boundaries and mean drop size for each of these atomization mechanisms. Both standard and flight orifice geometries are investigated. The data were obtained in both a static environment and in conventional aerodynamic facilities at Mach numbers of 4.5 and 8. The high-temperature aspects of reentry were simulated in a Mach 5.5 cyanogen-oxygen tunnel with total temperature of 4500 K.

17. Key Words (Suggested by Author(s))	18. Distribution Statement
Radio attenuation alleviation Drop size Water jets Light scattering Spray penetration	Unclassified – Unlimited

19. Security Classif. (of this report)	20. Security Classif. (of this page)	21. No. of Pages	22. Price*
Unclassified	Unclassified	53	$3.00

*For sale by the National Technical Information Service, Springfield, Virginia 22151

ATOMIZATION, DROP SIZE, AND PENETRATION FOR CROSS-STREAM WATER INJECTION AT HIGH-ALTITUDE REENTRY CONDITIONS WITH APPLICATION TO THE RAM C-I AND C-III FLIGHTS

By Paul B. Gooderum and Dennis M. Bushnell
Langley Research Center

SUMMARY

Atomization, drop-size, and penetration data are presented for cross-stream water injection at conditions simulating high-altitude reentry (low Weber number, high static temperature, high Knudsen number, and low static pressure). These results are applied to the RAM C-I and C-III flights. Two primary breakup modes are considered, "vapor pressure" or "flashing" and aerodynamic atomization. Results are given for breakup boundaries and mean drop size for each of these atomization mechanisms. Both standard and flight orifice geometries are investigated. The data were obtained in both a static environment and in conventional aerodynamic facilities at Mach numbers of 4.5 and 8. The high-temperature aspects of reentry were simulated in a Mach 5.5 cyanogen-oxygen tunnel with total temperature of 4500 K.

INTRODUCTION

The RAM (Radio Attenuation Measurements) series of flight experiments were designed by the Flight Instrumentation Division, Langley Research Center, to investigate the communications blackout phenomenon associated with high-speed reentry into the earth's atmosphere. These flight investigations have included measurements of the plasma parameters and techniques for alleviating the blackout problem. The results of the flight tests and of ground-based analysis and tests performed in support of the flights have been previously described. (See ref. 1 and the list of references therein.) One of the techniques studied for alleviating blackout has been that of injecting liquids (usually water) into the vehicle flow field (ref. 2). The evaluation of the results from these experiments requires accurate predictions of the liquid-spray parameters. Of particular importance are: (1) the determination of when and how the liquid jet breaks up (what is the boundary between breakup and no breakup), and (2) what is the mean drop size resulting from this breakup.

For the high-altitude (>60 km) portion of the RAM experiments (refs. 1 and 3), a high-velocity external airflow exists, which is at very low densities and pressures. The

local ambient pressure may be less than the vapor pressure of the liquid and as a result, there may be vapor pressure or flashing atomization of the injected water (ref. 4). At the lower altitudes, where the dynamic pressure of the airflow becomes large enough (i.e., greater than some critical value), aerodynamic breakup will occur (refs. 5 and 6). It will be shown for the RAM C-I and C-III flight trajectory that both breakup modes, aerodynamic and vapor pressure, occur separately over certain altitude ranges, and that they occur cooperatively in an overlapping altitude range.

Although liquid jet atomization, both in the presence of external gas flow or in quiescent ambient conditions, has been the subject of a considerable number of investigations, no studies have been made of liquid-jet-breakup—no-breakup boundaries at the high-altitude conditions of the RAM C-I flight. Most of the previous work on vapor-pressure breakup is contained in references 3 to 9 of reference 7. The literature on aerodynamic atomization has been primarily directed towards the study of droplet breakup (shattering of individual drops) with considerably less research concerned with jet breakup. (See ref. 8 and the list of references therein.) Virtually all these published results involve low Knudsen number conditions.

For the aerodynamic breakup—no-breakup boundary, there is ample theoretical and experimental evidence (refs. 9, 10, and 11) to indicate that Weber number, which is the ratio of the dynamic pressure of the gas flow to the surface-tension pressure of the liquid, is useful as a correlating parameter. The question arises as to whether this critical Weber number concept can also be applied to the high Knudsen number, high-altitude conditions of flight (low density, high static temperature).

Previous investigations of drop size from aerodynamic breakup have been mainly conducted at subsonic speeds (ref. 12). Only three investigations have been conducted at supersonic speeds (refs. 13, 14, and 15), none of which were at the low densities of interest for plasma electron concentration suppression.

Therefore, a research program was implemented and directed towards establishing the boundaries of the two primary modes of breakup and the determination of the resulting particle sizes once breakup occurred. This meant a twofold program involving both a static environment to study vapor-pressure effects alone and a wind-tunnel program with cold injection to minimize flashing effects (ref. 4). Also of interest, in the consideration of water injected from blunt vehicles reentering at high altitudes, is the question of possible effects of locally high static temperatures (ref. 16). Hence, aerodynamic breakup in both hot and cold environments was considered. Portions of the present study concerned with results obtained using standard research orifice configurations have been published in references 4, 7, 8, and 17. The present paper presents atomization and particle-size information for vapor-pressure atomization using the RAM C-I and C-III orifices and applies the accumulated research results to the conditions of the RAM C-I

and C-III flights. Additional drop size, aerodynamic atomization, penetration, and correlation of drop-size data are presented for the standard research orifice configurations as are experimental details not previously published. All results are for water injection normal to the airflow.

The development of the experimental program is indicated by the following table:

Facility	Vapor-pressure breakup boundary	Aerodynamic breakup boundary	Drop size	Penetration
Bell jar	X		X	
Cyanogen-oxygen tunnel		X	X	X
Mach 8 tunnel			X	X
UPWT		X		X

SYMBOLS

a,c,e	nozzle dimensions (see fig. 3)
b	nozzle dimensions (see fig. 1)
d_o	orifice exit diameter
D	vehicle nose diameter
D_{30}	volume mean drop diameter
D_{32}	volume to surface mean drop diameter (Sauter mean diameter)
f	focal length of receiving lens
I	light intensity
I'	light intensity due to slit scattering (see appendix)
I_o	light intensity without spray

K_n	Knudsen number, $\frac{M}{R}\left(\frac{\gamma\pi}{2}\right)^{1/2}$
L	orifice length
M	Mach number
N	number of injection orifices
p	pressure
$p_{t,2}$	pitot pressure
r	radius from center of point source image
R	Reynolds number, $\frac{\rho_g V_g d_o}{\mu}$
s	length of slit
S	slit length parameter, $\frac{s\pi D_{32}}{\lambda f}$
T	temperature
V	velocity
W_e	Weber number, $\frac{\rho_g V_g^2 d_o}{2\sigma}$
W_L	liquid Weber number, $\frac{\rho_L V_g^2 d_o}{\sigma}$
x,y	Cartesian coordinates along and normal to nozzle axis, respectively; origin at injection site
α	injection angle (relative to local vehicle surface)
γ	ratio of specific heats
Δ	shock layer thickness
ϵ	surface roughness height

θ	scattering angle, radians
λ	wavelength
μ	viscosity
ρ	density
σ	surface tension

Subscripts:

a	local static
amb	ambient
beam	scattering light beam
C.L.	center line
crit	critical
e	effective
g	gas
H_2O	water
L	liquid
max	outer spray limit, local
s	shatter
S.L.	streamline
t	stagnation

APPARATUS AND PROCEDURE

The experimental data for this investigation were obtained from both static bell-jar experiments and wind-tunnel tests in the Langley Mach 8 variable-density hypersonic tunnel, the high Mach number test section of the Langley Unitary Plan wind tunnel (UPWT), and a Mach 5.5 cyanogen-oxygen tunnel. The first problem to be considered will be the determination of the transition region between jet breakup and no breakup for both static and dynamic environments. This region will be referred to as the "breakup boundary."

Determination of Breakup Boundary

Static environment.- To evaluate the atomization behavior of water jets in the vapor-pressure mode of breakup, research was conducted in the static environment of an evacuated bell jar. Some of the experimental details have been previously reported (ref. 4).

Figure 1 shows the experimental setup and the basic orifice configurations used, both standard and RAM C-I, along with pertinent dimensions. The liquid delivery system consisted of a water container pressurized with nitrogen gas, and associated piping to connect the water container with the orifice. The water was injected into a large glass cylinder capable of being evacuated to 2 torr (267 N/m^2) during injection. The connecting piping was routed through a heated oil bath and a steam jacket so that the temperature of the injected water could be varied. The spray temperature was measured under vacuum by inserting a mixing cup equipped with a thermocouple into the flow immediately below the spray orifice.

It will be shown in the following section on the aerodynamic breakup boundary that at high-altitude conditions, for $W_e \leq 4$, no aerodynamic breakup is possible. Because of the low Weber number of these bell-jar tests $(W_e < 5)$, aerodynamic breakup effects are negligible and vapor-pressure atomization effects are expected to predominate. As a result, for external static pressures higher than the flashing or shatter pressure, a straight, well-formed cylindrical stream was obtained for each of the spray nozzles investigated. For the multiple orifice RAM-type nozzles, the multiple streams attached to one another at very low injection pressures and appeared to behave as a single jet. At higher injection pressures $(p_L > 10^5\ N/m^2)$, the multiple streams remained separated. Otherwise, they appeared to behave as did the single orifice nozzles, with a definite shatter pressure for each temperature.

When the pressure in the bell jar dropped below a certain value, the jet or jets disintegrated. This disintegration pressure was found to be a function of the injectant temperatures. The test procedure was to heat the flowing spray water to the desired temperature and then lower the pressure in the bell jar until flashing occurred. This pressure

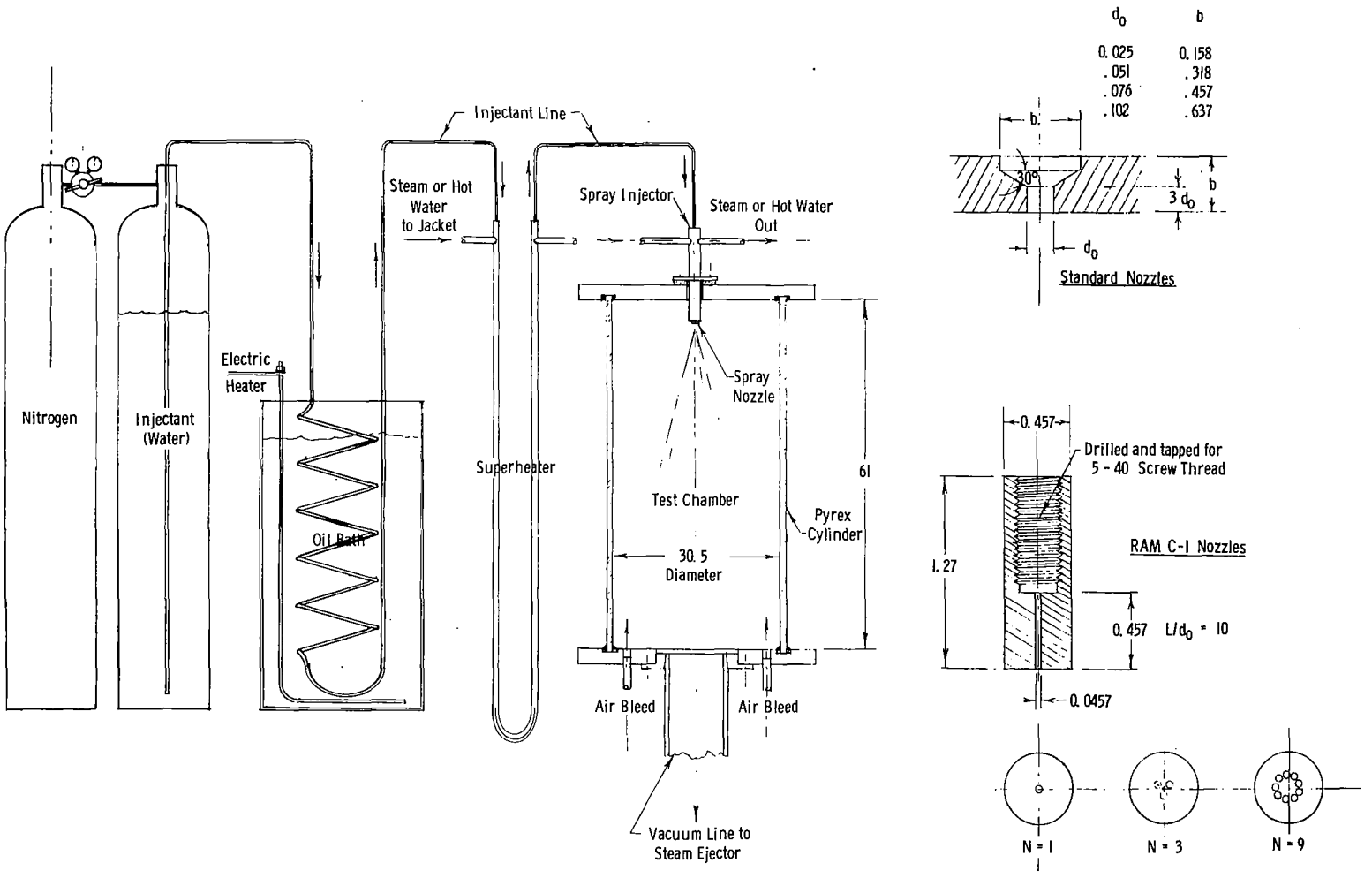

Figure 1.- Schematic drawing of vacuum-chamber equipment used to determine vapor-pressure breakup boundary (static environment). All dimensions in centimeters.

could be detected only with a limited degree of accuracy. Therefore, there is some uncertainty in the shatter pressure. This corresponded to an uncertainty in shatter temperature, at any given ambient pressure, of ±6 K. Consequently, the breakup data show scatter about a mean value. Photographs of a typical flashing jet are shown in figure 2 for d_o = 0.0508 cm. Jet flashing occurred at pressures below 20 torr (2.7 kN/m^2) for this series of pictures.

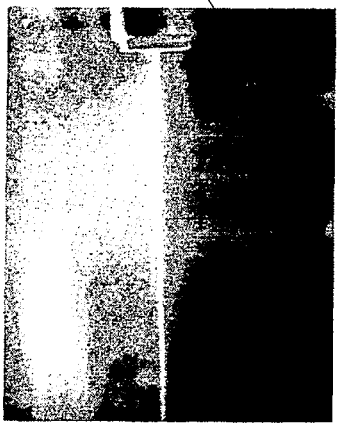

(a) p_a = 50 torr (6.7 kN/m^2).

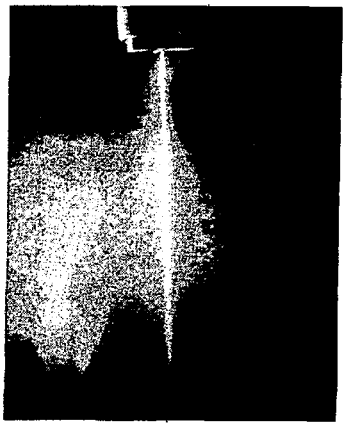

(b) p_a = 27.5 torr (3.7 kN/m^2).

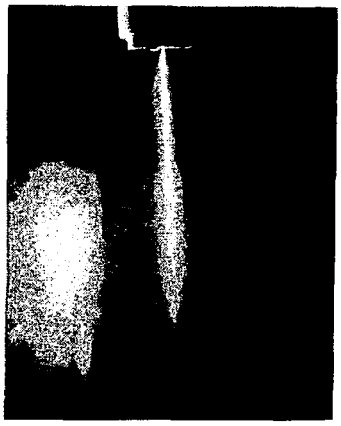

(c) p_a = 15 torr (2.0 kN/m^2).

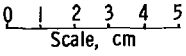

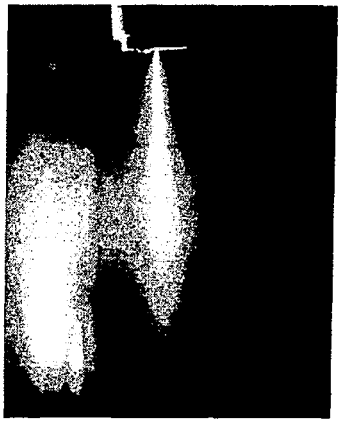

(d) p_a = 10.5 torr (1.4 kN/m^2).

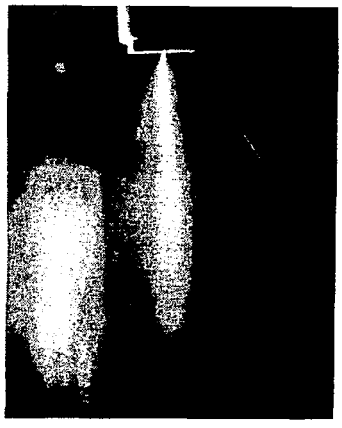

(e) p_a = 6 torr (0.80 kN/m^2).

L-72-2415

Figure 2.- Photographs of vapor-pressure breakup in bell jar. d_o = 0.0508 cm; standard nozzle; T_L = 330 K.

Aerodynamic environment.- In order to provide more confidence in the use of a critical Weber number atomization criterion at high Knudsen number K_n, it was necessary to obtain additional experimental data. To simulate experimentally a water jet at its critical Weber number condition on a vehicle reentering the earth's atmosphere over an altitude range of 75 to 40 km, a series of liquid-jet breakup tests were run in a Mach 5.5 cyanogen-oxygen tunnel. This apparatus (as well as the standard orifice configuration, along with pertinent dimensions) is shown in figure 3. The facility utilizes a stoichiometric cyanogen-oxygen combustion reaction, with a flow rate of about 32 g/s to produce a 20-cm-diameter axisymmetric stream consisting of a mixture of two parts CO and one part N_2 at a stagnation pressure of 1 atmosphere and a stagnation temperature of 4500 K. The facility was designed to simulate values of the local gas dynamic parameters which are encountered along the afterbody of a blunted configuration traveling at near orbital speeds. Parameters simulated and typical experimental values for Mach 5.5 operation are: Velocity, 3000 m/s; static temperature, 825 K; and static pressure, 0.48 torr (64 N/m^2). A variable Weber number was obtained by varying the diameter of the liquid-spray orifice.

Since this facility has a conical nozzle, it produces a longitudinally varying Mach number ($\approx$5.4 to 5.6) and static density (2.5 to 2.0×10^{-7} g/cm^3) over the region in which the spray is observed. Facility calibration results are shown in figure 4 which indicate a fairly uniform core, approximately 13 cm in diameter. The relative surface roughness of the spray orifices (ϵ/d_o) as estimated by microscopic examination was $\leq$0.01. In order to minimize vapor-pressure breakup effects, the spray water was injected cold, at 4^o to 8^o C. By an extrapolation of the vapor-pressure breakup data of reference 4 to 1 torr (133 N/m^2) ambient pressure, the vapor-pressure-breakup—no-breakup boundary is determined to lie between 0^o and 5^o C for the particular orifices considered. To verify that the spray water was cold enough and therefore that aerodynamic breakup was the principal mechanism tending to atomize the jets, the test section was evacuated to 0.2 torr (27 N/m^2) and the jets operated without tunnel flow at the spray temperatures used for the runs with flow. The results verified the assumption of negligible vapor-pressure breakup for these aerodynamic breakup tests.

The liquid delivery system consisted of a water reservoir filled with crushed ice, at atmospheric pressure, connected to the spray orifices through jacketed supply lines. Refrigerant at 2^o C was circulated through the jackets and through coils in the ice bath.

It was found necessary to heat the ends of the spray nozzles to prevent ice accumulation on their outside surface with the possibility of its interference with the liquid spray and with the tunnel flow. This was done by soldering a copper tube to the sides of the nozzles and passing high pressure steam through it. The temperature of the injected liquid was monitored by means of thermocouples placed in the spray-water lines immediately upstream of the spray orifices. The short residence time in the heated nozzle was

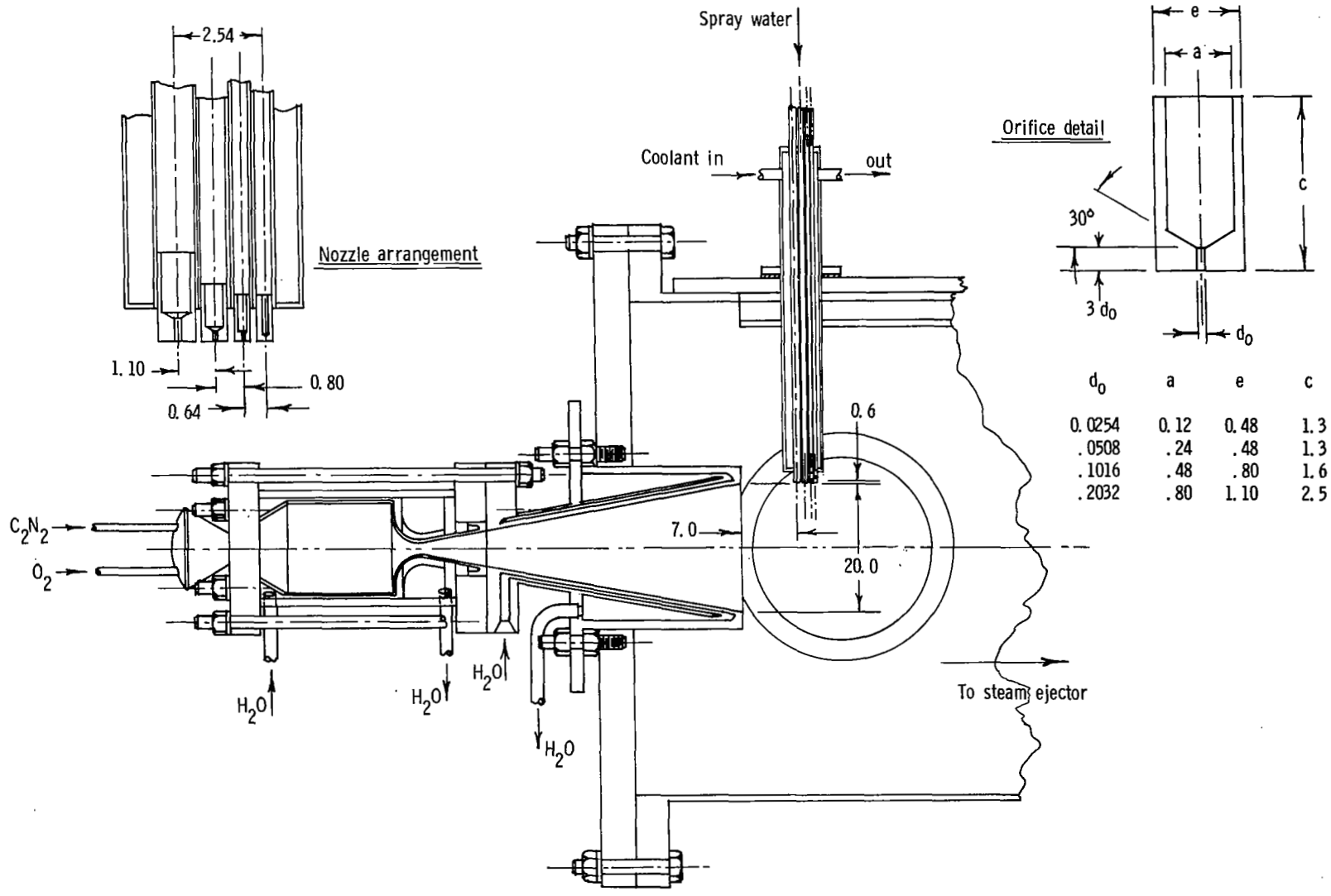

d_0	a	e	c
0.0254	0.12	0.48	1.3
.0508	.24	.48	1.3
.1016	.48	.80	1.6
.2032	.80	1.10	2.5

Figure 3.- Cross sections of cyanogen-oxygen facility and injection nozzles. All dimensions in centimeters.

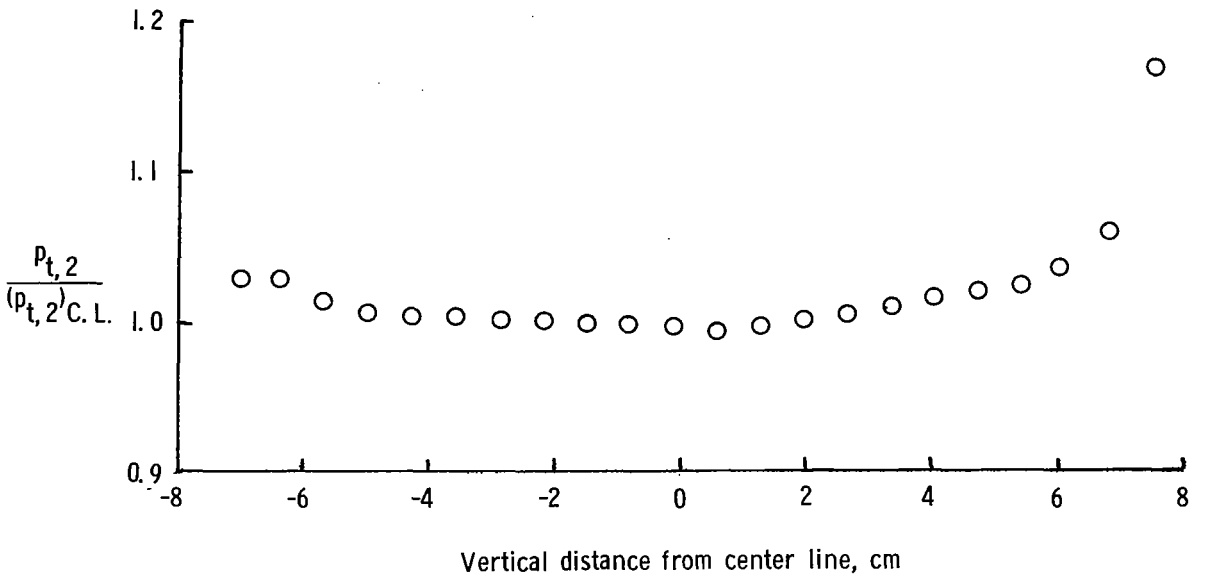

Figure 4.- Total-pressure survey 17.4 cm from nozzle exit.
Mach 5.5 cyanogen-oxygen tunnel.

not sufficient to warm the spray water appreciably. If operated for a long period of time, however, the steam heater was found to have an effect on the refrigerant temperature. For this reason, the time that the heater was operated was limited to the time required for nozzle operation.

Photographs of the spray were made with 16-mm and 70-mm cameras. Illumination of the spray was furnished by light from the combustion chamber passing through the throat of the wind-tunnel nozzle. Figure 5 is a reproduction of four frames from the 16-mm film showing the spray from the orifices with diameters of 0.0254, 0.0508, 0.1016, and 0.2032 cm. The indistinct appearance of the lower portion of the smallest jet (0.0254-cm-diameter) is due to a small amount of breakup plus small fluctuations in the position of the liquid stream which were caused by variations in tunnel static and stagnation pressures. For the purpose of this investigation, however, this small jet was considered to be unbroken since the first few centimeters of liquid stream appeared quite coherent to the unaided eye.

In order to investigate the variation of $W_{e,crit}$ between $K_n = 10^{-5}$ and 1.0 and establish with certainty whether or not there is any effect of Knudsen number on the breakup—no-breakup boundary (ref. 8), additional wind-tunnel data were obtained in the Langley Unitary Plan wind tunnel operated at its highest Mach number (M = 4.6) and lowest stagnation pressure $\left(p_t \approx 80\ kN/m^2\right)$. This produced $W_e = 7.6$ at $K_n = 2 \times 10^{-2}$ for $d_o = 0.0127$ cm.

(a) d_o = 0.0254 cm; T_{H_2O} = 6.7° C; p_{H_2O} = 1 atm (101 kN/m^2); V_{H_2O} = 14.3 m/s; W_e = 3.9.

(b) d_o = 0.0508 cm; T_{H_2O} = 7.8° C; p_{H_2O} = 0.97 atm (98 kN/m^2); V_{H_2O} = 14.0 m/s; W_e = 8.3.

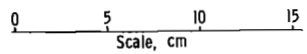

(c) d_o = 0.1016 cm; T_{H_2O} = 5.6° C; p_{H_2O} = 0.88 atm (89 kN/m^2); V_{H_2O} = 13.4 m/s; W_e = 15.7.

(d) d_o = 0.2032 cm; T_{H_2O} = 4.4° C; p_{H_2O} = 0.61 atm (62 kN/m^2); V_{H_2O} = 11.2 m/s; W_e = 31.4.

L-72-2416

Figure 5.- Photographs of spray in Mach 5.5 cyanogen-oxygen tunnel. N_2 + 2 CO flow; T_t = 4500 K; T_{amb} = 825 K; p_{amb} = 0.48 torr (64 N/m^2).

The basic configuration for the UPWT tests was a 46-cm-long flat plate alined with the free stream, with injection orifices 0.0127, 0.0254, 0.0508, and 0.1016 cm in diameter installed in the center of an 11-cm-diameter plug located 8.6 cm ahead of the trailing edge (see fig. 6). The remainder of the plumbing was identical to that used in the

L-72-2417

(a) Photograph of model mounted in test section.

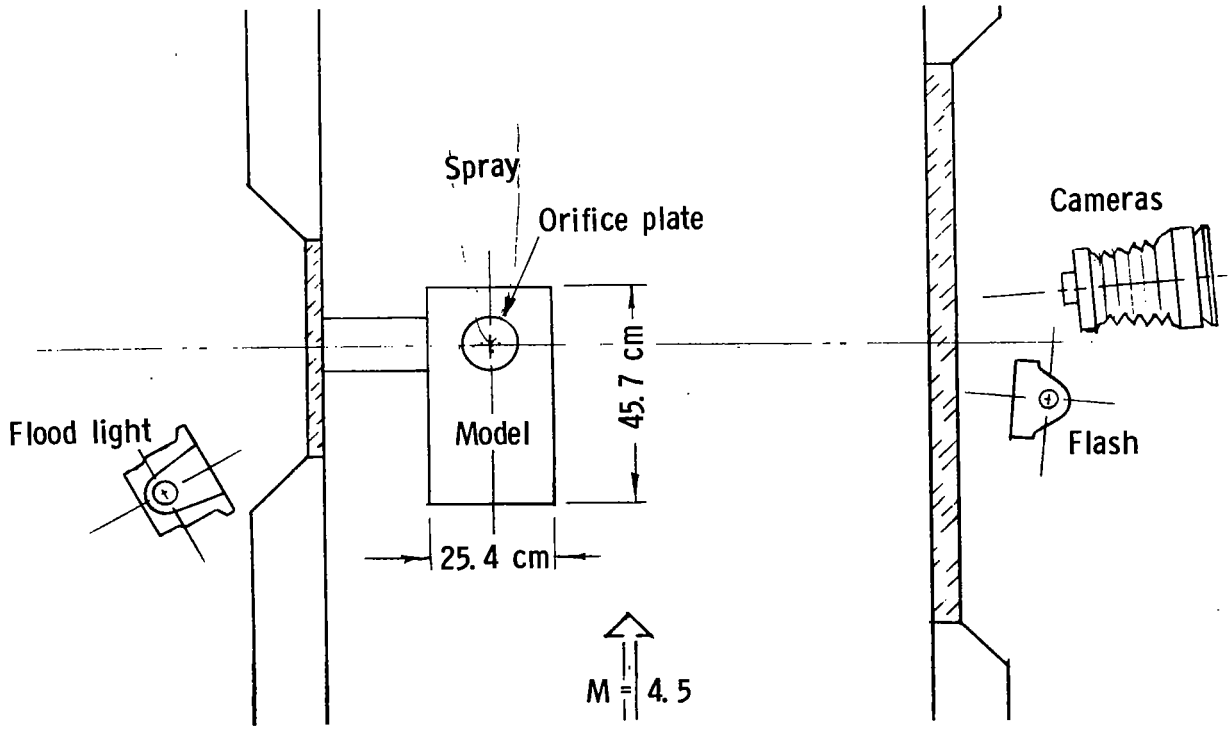

(b) Schematic drawing of test arrangement.

Figure 6.- Unitary Plan wind-tunnel model and location diagram.

cyanogen-oxygen tunnel. Two sources of illumination were utilized: First, the spray was photographed by placing a high-intensity photolight on the opposite side of the spray from the camera and the scattered light photographed by both motion-picture camera (32 frames per second) and still camera $\left(\text{Exposure} = \frac{1}{150}\ \text{s}\right)$. Second, a short-duration electronic flash was placed on the near side of the spray and another still photograph taken of the spray simultaneously with the others, using back-scattered light from the flash. This third photograph was taken to check the effect of shutter speed on the appearance of the spray and to determine to what extent apparent breakup is actually fluctuation in coherent jet position while the camera shutter is open. The tunnel was then operated over a wide range of conditions ($7.6 < W_e < 242$) so as to obtain data on both the aerodynamic breakup boundary and on penetration.

Determination of Drop Size

Static environment.- The authors knew of no previous measurements of drop size for atomized water sprays under the difficult conditions of our primary problem, that of injection into a high-velocity flow in a vacuum. After study of available particle-size measuring techniques, an optical method based on the small-angle diffractive scattering of light was selected which proved to be convenient and readily applied. This technique yields a mean diameter which is approximately the D_{32} (Sauter mean diameter) of the spray, provided the drop-size distribution can be approximated by the Upper Limit Distribution Function of reference 18. The resulting D_{32} is only weakly dependent on the shape of this function (ref. 19). The bell-jar and injection system previously described was modified to receive an optical system for the determination of drop size by measurements of small-angle light scattering. Previous investigators, in applying this technique, have used the photographic method (i.e., instantaneously obtaining the variation of intensity of the scattered light by placing a sheet of photographic film in the reception plane). The photographic technique was found to be quite laborious and subject to several additional sources of error (connected with photographic development techniques, film calibrations, etc.) as compared to the more direct photoelectric method. This later method, which utilizes a photomultiplier tube to scan the scattered-light pattern, is quite rapid, easily lending itself to automated data processing procedures. Some of the following experimental details have been previously reported (refs. 7 and 17).

A diagram of the light-scattering apparatus is shown in figure 7. The spray was illuminated by a parallel beam of monochromatic light 2.5 cm in width by 2 cm in height. The apparent source of light was a slit 0.05 cm wide and 2 cm long. The actual source was an air-cooled BH-6 mercury light operated at approximately 320 W power input, with a 4-cm-thick water filter to protect adjacent optical elements. An interference filter isolated the 0.5461-μm line and a light stop restricted the parallel beam traversing the spray. The collimating and receiving lenses were identical: 62.6-cm focal length and

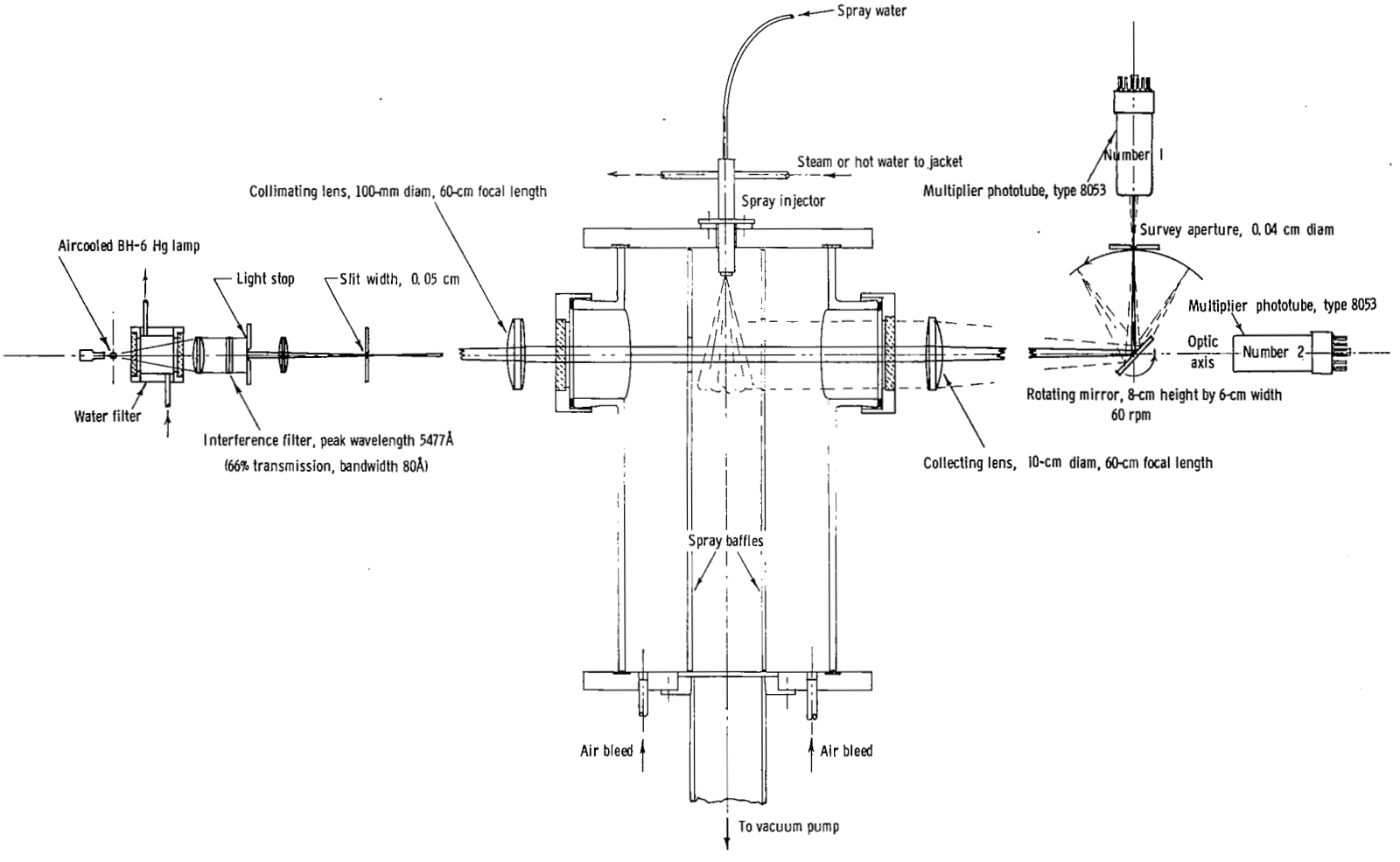

Figure 7.- Sketch of light-scattering apparatus used for mean drop-size measurements in vacuum chamber (bell jar).

10-cm diameter. The light receiver consisted of an 8053 photomultiplier tube placed 5 cm behind a survey aperture of 0.04-cm diameter.

The light-intensity variation along a line perpendicular to the slit image and the optic axis was determined by sweeping the image of the slit source, formed by the receiving lens, past the pinhole photomultiplier radiometer by means of a 60-rpm rotating mirror. To reduce amplifier saturation effects caused by the passage of the direct unscattered central light image past the photomultiplier, it was found necessary to limit the intensity of the light source. As a result, the point source of light, required by theory, proved to provide too low a signal-to-noise ratio for all but the most dense sprays. A slit source was therefore substituted for the conventional point source, since the slit would furnish much more scattered light for the same spray and source intensity.

In order to obtain a mean drop size from an experimentally produced diffraction pattern, it is necessary to be able to compare the measured distribution with a theoretical or calibration curve. Since the only available theoretical distribution (ref. 18) is for a point source, the preferred procedure would have been to obtain a calibration distribution for a slit source from an experimental dispersion of known D_{32}. It is unfortunate that no such standard exists, either as a spray or as a group of particles distributed over a glass microscope slide. Hence, it was decided to calculate the requisite theoretical scattered-light profile. This profile was obtained by integration of the normalized diffraction pattern for a point source available from reference 18. (See the appendix.) The results of that integration showed very little practical difference between the theoretical profile for slit scattering and the original point-source profile from reference 18. Hence either profile could be properly used as a standard for comparison with the experimental data.

The following limitations then apply to the type of particulate dispersions which can be investigated:

(1) Only relatively large spherical particles are considered (drop sizes are much larger than 0.1 μm).

(2) It is assumed that the particles are of high refractive index relative to the adjacent medium.

(3) No refractive-index variations occur in the medium surrounding the drops.

(4) Although the frequency of occurrence of the various particle sizes of the dispersion does not necessarily have to agree with that predicted by the Upper Limit Distribution Function, there is assumed to be very little agglomeration since the scattered light is very strongly influenced by the presence of very large particles.

Experience with water has shown that violations of these limitations may not present any problems of importance since their transgression usually results in a distorted diffraction pattern. Any distorted patterns can be discarded.

The diffraction patterns for the experimental sprays were measured using the following procedure. The scattered-light signal from the photomultiplier was recorded at both high and low gain by photographing the signal on a dual-beam, dual-trace oscilloscope, the sweep being triggered by a photocell placed to intercept the moving slit image as it approached the survey aperture. A third channel was set up to monitor the intensity of the central image, attenuated by a neutral density filter, and recorded at reduced sweep speed by means of a second photomultiplier looking directly into the optical system. Twice each revolution of the rotating mirror, at the time the mirror becomes parallel to the optic axis, this phototube gets a partially obstructed view of the light-source image which can then be used to measure the attenuation of the light beam by the fog. This attenuation measurement is useful as a means of determining the extent to which multiple scattering is occurring. The transmitted light intensity through the fog should be no smaller than 25 percent of that transmitted in the absence of fog (ref. 18).

The test chamber was the same 30.5-cm- by 61-cm-long glass cylinder used to determine the vapor-pressure breakup boundary. In this investigation, the cylinder was divided into three sections by two flat lucite baffles, extending the length of the cylinder, held 10 cm apart by spacers, with the only openings from one section of the cylinder to another being a 5-cm-diameter hole for the light beam on the approach-side baffle and a 10-cm-diameter hole for the light beam on the exit-side baffle, both openings being centered on the optic axis.

The glass jar was evacuated by means of a 7.5-cm-diameter vacuum line leading from the center section to a four-stage steam ejector. Bleed air moving through the holes in the baffles prevented the transfer of fog into the outside sections which would condense on the windows. The rate of bleed was maintained low enough so that no disturbance of the spray was observed. With the water spray, bleed air, and steam-ejector vacuum system in operation, the lowest pressure attainable in the test section was approximately 2 torr (267 N/m^2). The various test pressures in the test section were reached by throttling the flow to the steam ejector, simultaneously adjusting bleed-air flow to the desired rate. For this part of the investigation, the spray-water temperature was measured continuously by means of a thermocouple inserted into the spray water immediately upstream of the orifice.

The run procedure included making a scattering record without spray (see fig. 8(a)) and then a minute or so later, after the spray-water temperature and bell-jar pressure have become adjusted to the desired values, a second and third record with spray (see fig. 8(b)). The scattering angle is determined by measuring from the center of the pulse caused by the passage of the central slit image past the survey aperture and recorded by the low-gain trace. The actual scattered-light data are the lower traces in the figure, where a deflection in the upward direction represents an increase in light flux through the survey aperture caused by the increase in light level as the slit image approaches the

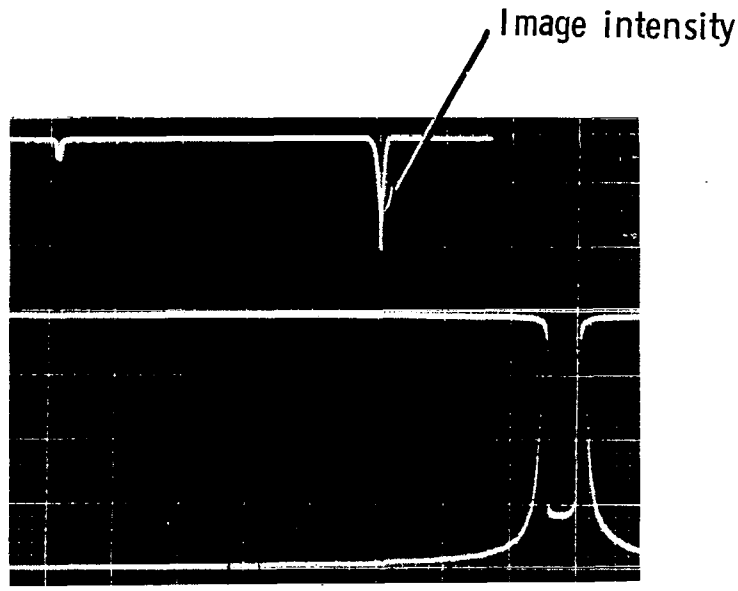

(a) Without spray.

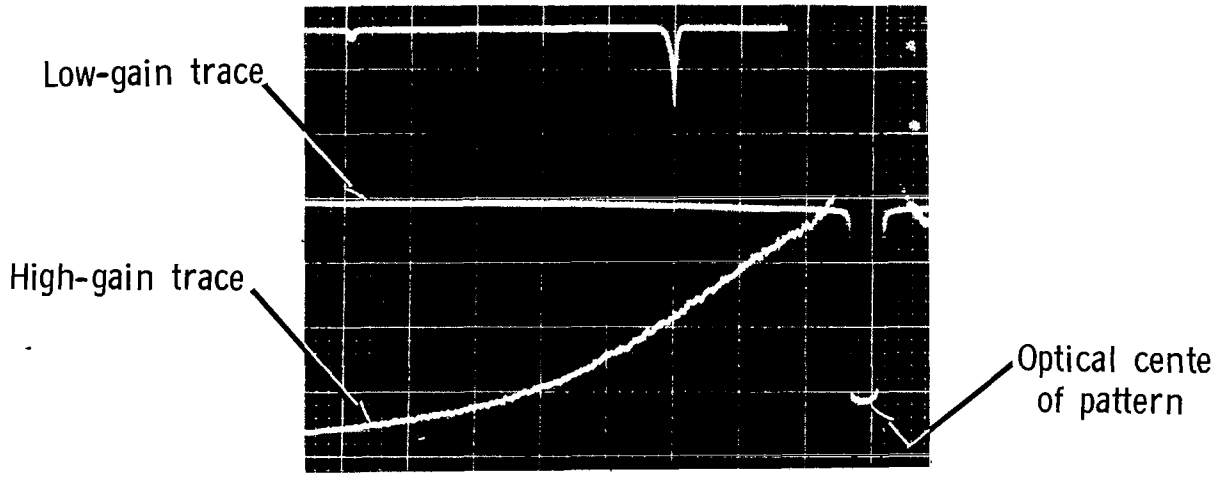

(b) With spray.

Figure 8.- Typical light-scattering records. (Principal data are the lower traces in each photograph.)

aperture. The difference in height of the lower trace between the photographs (see fig. 8) is assumed to be that due to the actual scattering caused by the spray; that is, the total scattering less that caused by the fixed components of the system such as windows and lenses.

The data-reduction procedure was to take the measured scattered-light intensity from the spray record I and subtract the background light due to the optical system I_o. The difference is then plotted against the scattering-angle parameter $\pi\theta/\lambda$ (see fig. 9).

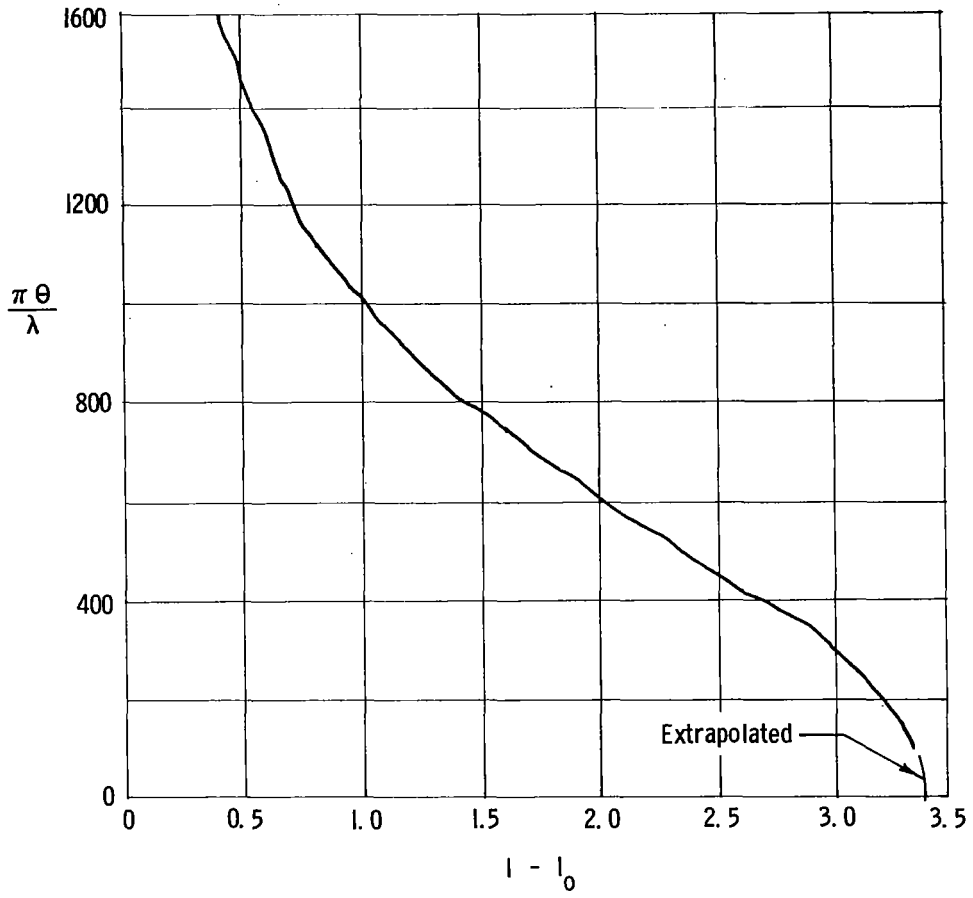

Figure 9.- Plot of light scattering by water spray against scattering-angle parameter $\pi\theta/\lambda$.

This plot was then graphically extrapolated so as to intersect the center line of the diffraction pattern $\left(\frac{\pi\theta}{\lambda} = 0\right)$ with zero slope. This center-line value of the light intensity $(I - I_o)_{C.L.}$ was then used to obtain a nondimensional intensity distribution $\frac{I - I_o}{(I - I_o)_{C.L.}}$ as a function of the scattering-angle parameter $\pi\theta/\lambda$. The D_{32} for the spray was then obtained by comparing these data with the standard nondimensional illumination curves for slit scattering $I'(\theta)$ plotted against $\pi\theta/\lambda$ for various values of D_{32}. The value of D_{32} assigned to a given spray pattern is that which gives the best fit over the most meaningful portion of the curve, which was generally $0.7 > \frac{I - I_o}{(I - I_o)_{C.L.}} > 0.2$. A typical

comparison of this type is shown in figure 10. The D_{32} value assigned to this particular spray (d_o = 0.0254 cm; p_a = 89 torr (11.9 kN/m^2); p_L = 590 kN/m^2; T_L = 101° C) was 20 μm.

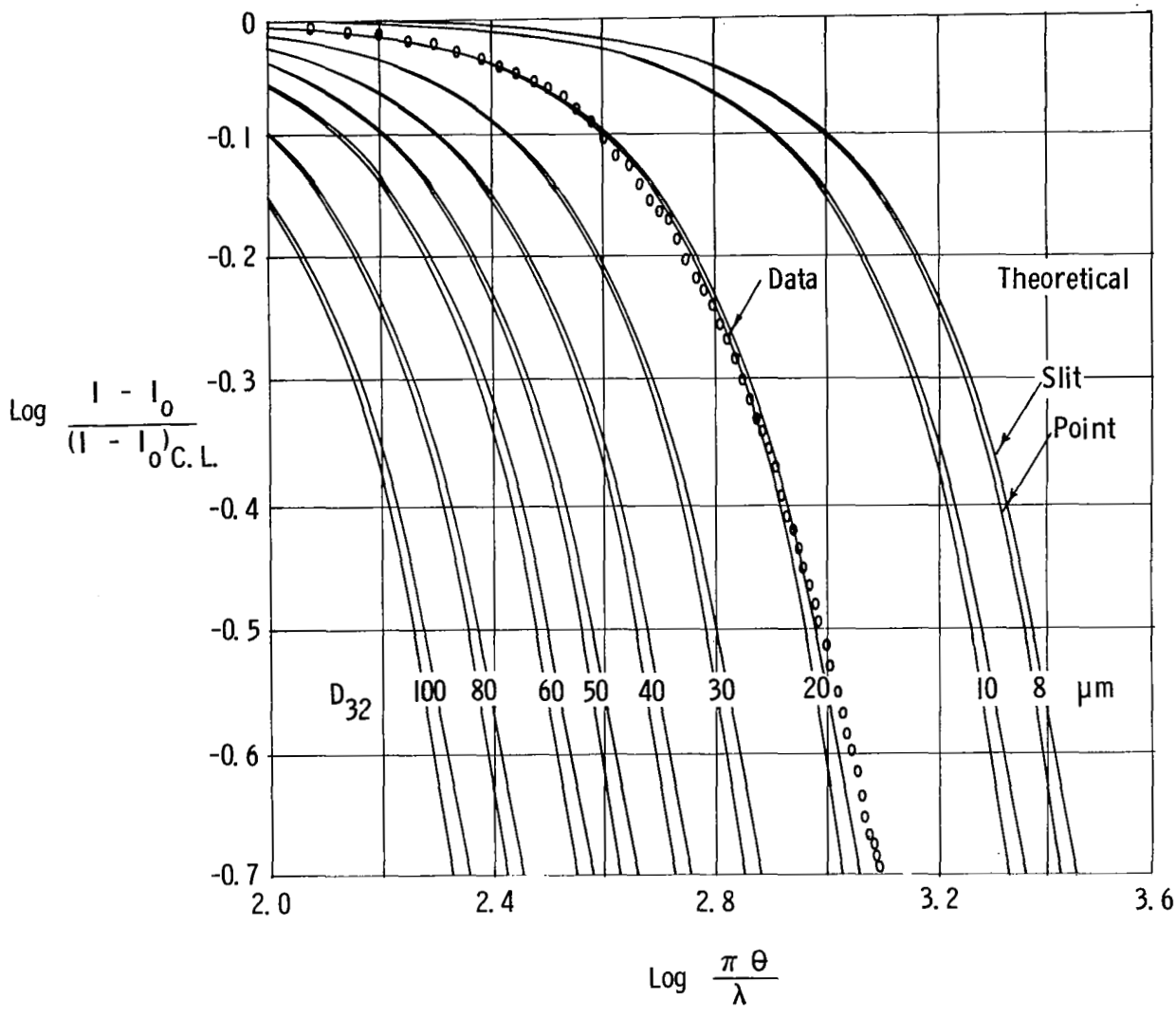

Figure 10.- Volume to surface mean drop-size determination by comparison of experimental scattered-light intensity distribution with theoretical distributions for both point source and slit source.

Aerodynamic environment.- The investigation of drop size due to aerodynamic breakup was conducted in both the Langley Mach 8 variable-density hypersonic tunnel and a Mach 5.5 cyanogen-oxygen tunnel. A sketch of the flat-plate model used in the Mach 8 tests is shown in figure 11. The injection orifice was installed on the center line of the model (and of the tunnel) 7.62 cm back of the leading edge, as shown. Details of the orifice along with the range of d_o values and corresponding L/d_o ratios are given in the figure.

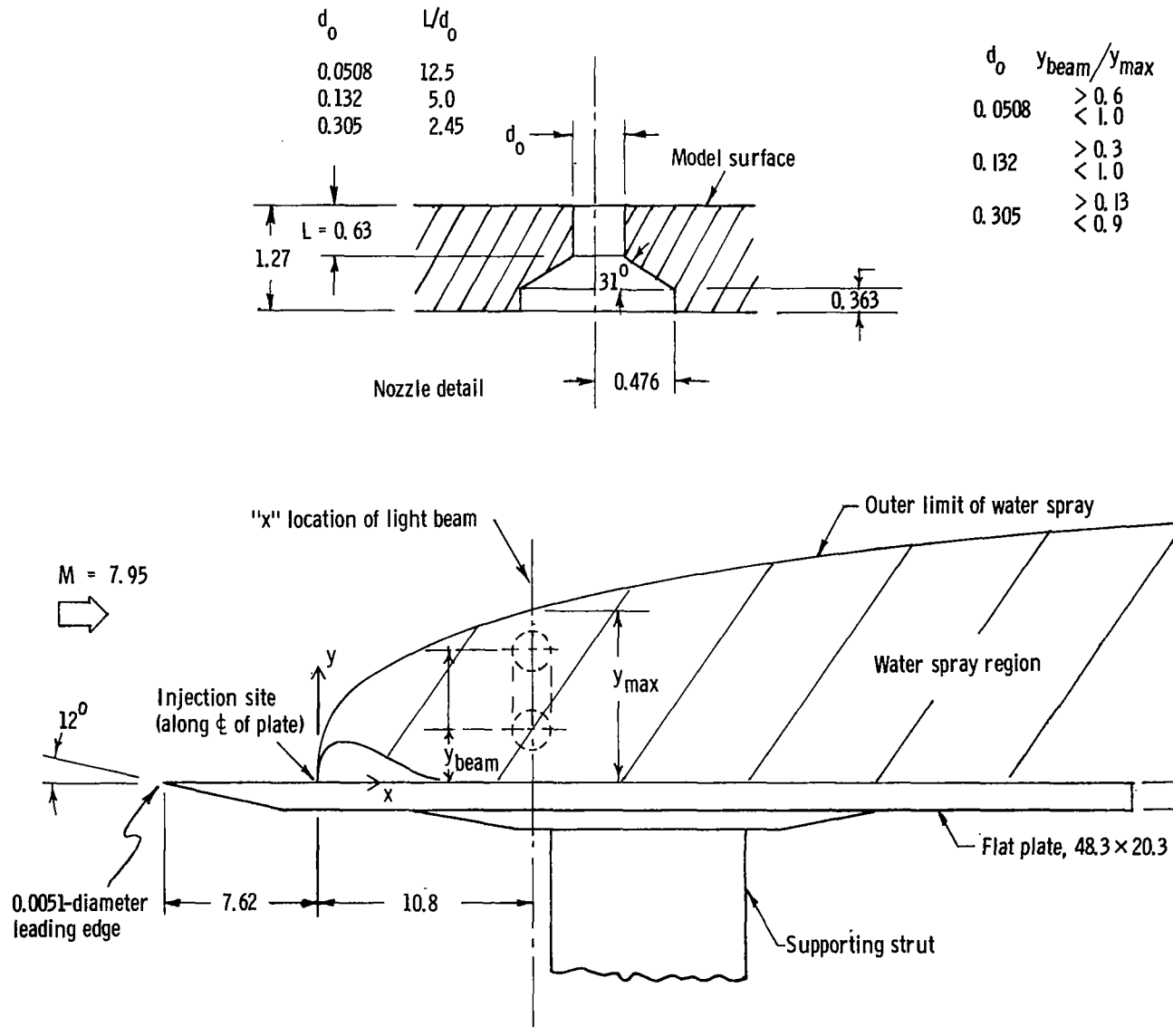

Figure 11.- Sketch of model and injection orifices, Mach 8 water-injection study. Dimensions are in centimeters.

The determination of the mean drop size of the spray was accomplished by means of the same small-angle light-scattering technique (and therefore the same optical apparatus) described in the previous section on vapor-pressure breakup. The wind-tunnel test section was 45 cm in diameter with 30-cm-diameter schlieren quality windows 3.2 cm thick. The model span was 20.3 cm. The test-section pressure was varied over the range of 0.5 to 5 torr (67 to 670 N/m^2). Stagnation temperatures were approximately 800 K. A total of 55 runs were made, each lasting an average of about 20 seconds. Forty of these were for light-scattering drop-size determination and 15 for scattered-light screen photographs of the spray patterns, to be used for penetration measurements. In a typical drop-size determination, two or three diffraction patterns with water injection were recorded along with an identical diffraction pattern without spray. Measurements of mean drop diameter were obtained only at $x = 10.8$ cm. Data were obtained at various y-positions in the spray by adjusting the height to which the model was inserted. Figure 12 shows typical photographs of the water spray taken with scattered light from a floodlight placed on the far side of the tunnel from the camera.

In order to determine the effects of flight conditions at high altitude on drop size, the aerodynamic breakup tests were repeated in a Mach 5.5 cyanogen-oxygen tunnel (see fig. 13) using the spray system from the vapor-pressure breakup studies in the bell jar, injecting directly into the stream from an orifice external to the flow (see fig. 3). The light-scattering apparatus was modified to adapt the system towards meeting problems peculiar to the cyanogen-oxygen tunnel. To eliminate scattered light caused by light from the combustion chamber, the interference filter was moved from the light source to the survey aperture. Other modifications included changing the survey aperture from a pinhole (0.04-cm-diameter) to a slit (0.0057-cm-wide by 0.64-cm-long, installed with long axis parallel to long axis of source image) to obtain better pattern resolution and higher signal level, and installing protective tubes around the scattering beam within the test section. These tubes had an atmospheric air bleed directed against the inside of the test-section windows to prevent window fogging and to sweep any spray external to the cyanogen-oxygen jet out of the tubes and light beam. In addition, the spray injector, which was the same one used in the aerodynamic breakup-boundary investigation, was rotated about its axis so that the line of orifice centers was perpendicular to the tunnel axis. This orientation was needed because it was desirable to compare the mean spray drop size at identical points in the spray pattern. To obtain equal penetrations for the four orifices (0.0254, 0.0508, 0.1016, and 0.2032 cm in diameter), it was required to increase the injection pressure as the size of the orifice was decreased. To determine the injection pressure required, an initial penetration study was conducted, wherein the spray penetrations for the four orifices were photographed for various injection pressures varying from 0.67 to 52 N/m^2 for an ambient pressure of approximately 1 torr (133 N/m^2) ($T_L = 17^o$ C).

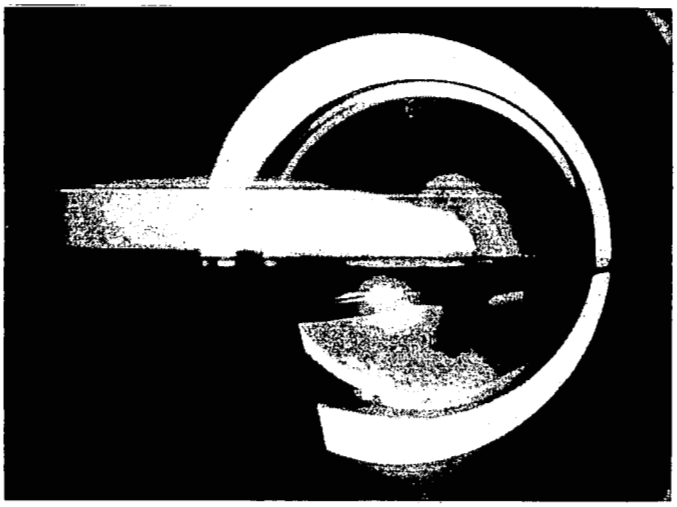

(a) $W_e = 118.2$; $d_o = 0.0508$ cm; $\sqrt{\frac{\rho_L V_L^2}{\rho_g V_g^2}} = 10.$

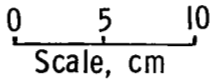

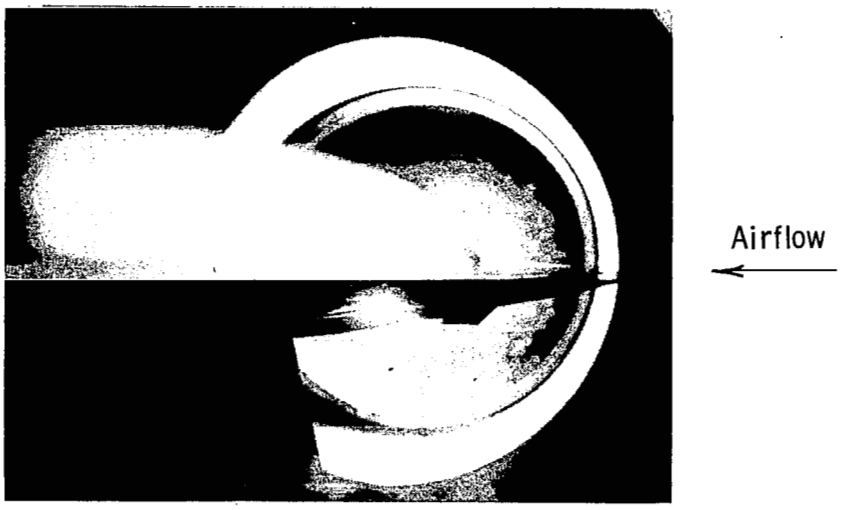

(b) $W_e = 1266$; $d_o = 0.3048$ cm; $\sqrt{\frac{\rho_L V_L^2}{\rho_g V_g^2}} = 4.9.$

L-72-2418

Figure 12.- Spray photographs from tests in the Mach 8 variable-density tunnel.

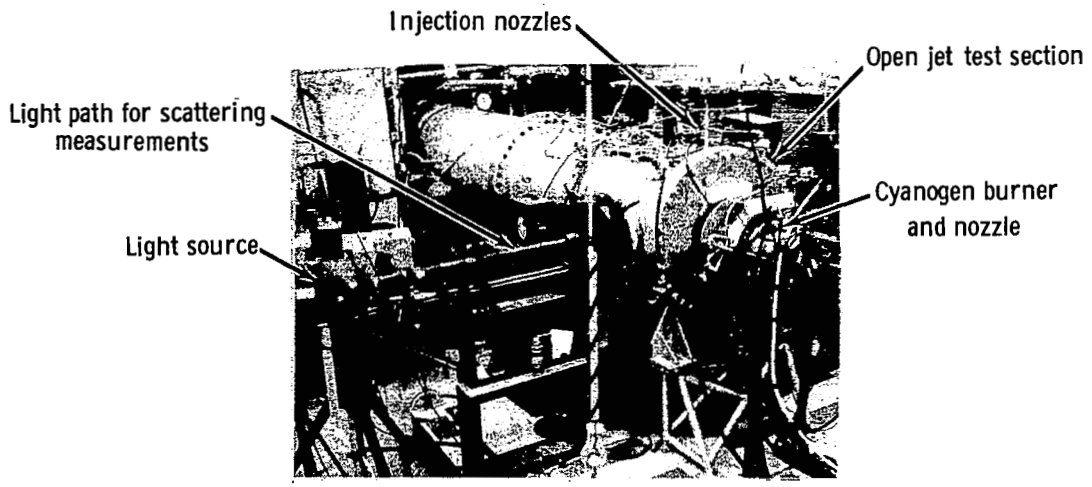

L-72-2419

(a) Photograph of test apparatus.

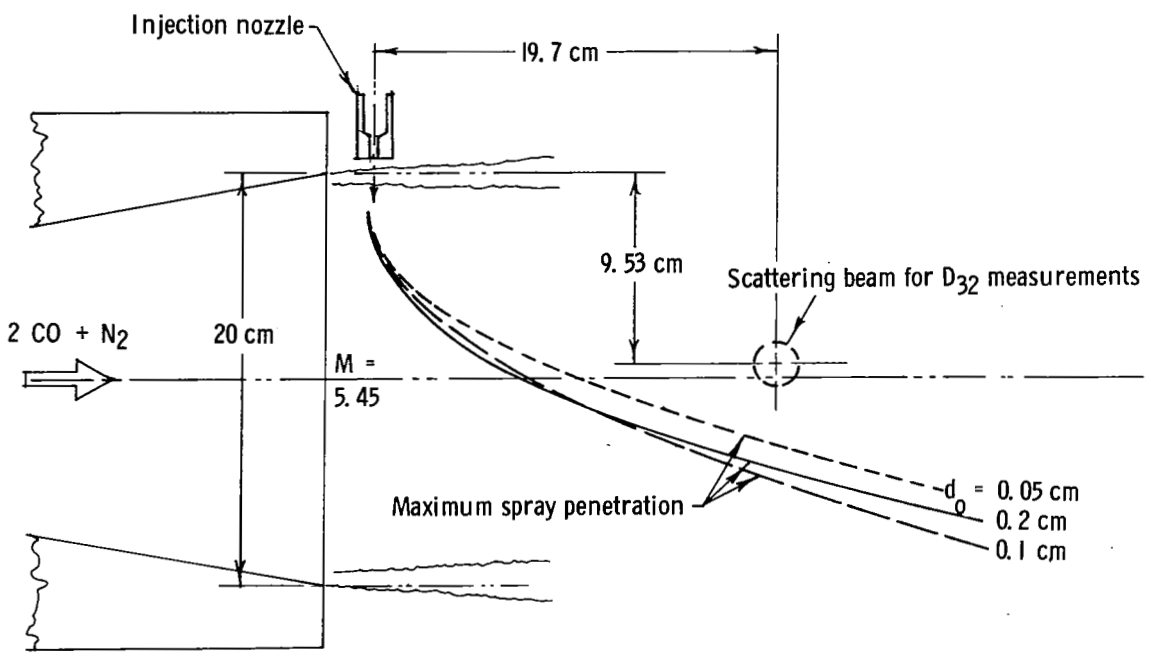

(b) Position of scattering beam for mean drop-size measurements.

Figure 13.- Physical setup for mean drop-size measurements in cyanogen-oxygen facility.

The procedure was to inject downward, perpendicular to the flow on the nozzle axis, from the series of four injectors with a nominal location 2.2 cm out and 0.64 cm up from the end of the nozzle and the edge of the gas flow. The location of the scattering beam was at $x = 19.7$ cm downstream and $y = 9.53$ cm down, referenced to the point where the water jet entered the gas stream. Figure 14 shows the spray patterns attained for a typical run, with the salient points diagramed in figure 13(b). The run procedure was as follows: a prerun scattered-light calibration pattern was first taken; followed by tunnel operation wherein three or four scattered-light diffraction patterns were obtained for each spray orifice; and immediately followed after tunnel shutdown by taking a postrun calibration pattern. The scattered-light data were coordinated with a motion-picture record of the spray (illumination provided by the combustion chamber) by means of a light flash triggered by operation of the scope camera shutter. The intensity of the light source for the light-scattering system was monitored by a separate photocell. Brightness variations were corrected by manually adjusting the power supply as they occurred.

Drop-size data were obtained for two different spray temperatures, $T_L = 19^{\circ}$ and 2° C, to determine what effect, if any, vapor-pressure breakup may have on the resulting mean drop size.

RESULTS OF GROUND RESEARCH

Breakup Boundary

Static environment.- Some of the experimental results of this part of the investigation (the breakup—no-breakup boundary for flashing water jets in a static environment) have been previously reported in reference 4 for the standard research orifice configuration. The complete set of resulting data are shown as data bands in figures 15(a) and 15(b). New data for the RAM C-I injection nozzles are shown as data points in figure 15(c). The vapor-pressure relationship for water (uppermost curve) is presented on each figure as a location of reference. Figures 15(a) and 15(b) summarize the results of reference 4 for the breakup boundaries of the standard orifices. As can be seen, the smaller diameter orifices required a larger amount of "superheat" (25 to 30 K) before flashing occurred (see fig. 15(a)). The larger nozzles (see fig. 15(b)) required less superheat (15 to 20 K) to shatter the liquid jet. This difference in required superheat between the two sets of nozzles was ascribed in reference 4 to the presence of two-phase flow within the nozzle itself for the larger orifices. As the L/d_o is the same for all standard nozzles, the longer length and greater surface area available to support nucleation sites may be the reason for the possible presence of two-phase flow within the larger nozzles (see also ref. 20).

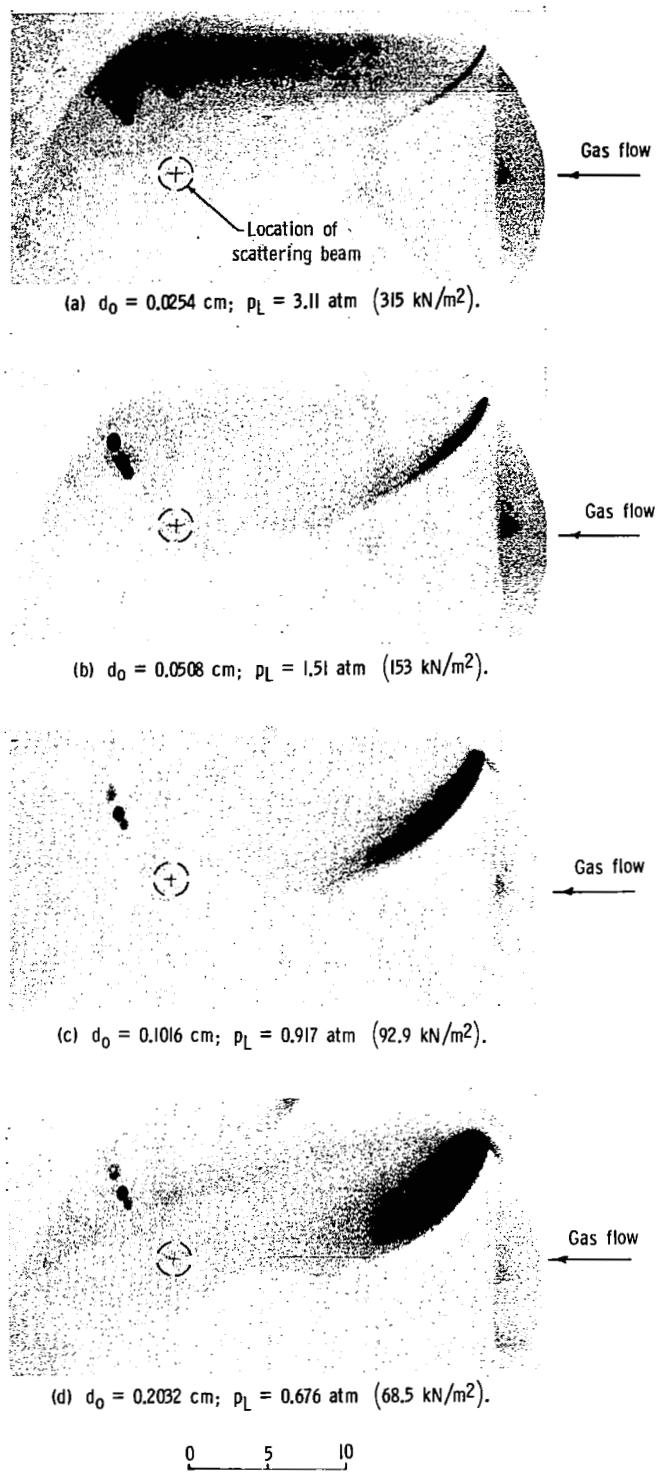

(a) d_0 = 0.0254 cm; p_L = 3.11 atm (315 kN/m^2).

(b) d_0 = 0.0508 cm; p_L = 1.51 atm (153 kN/m^2).

(c) d_0 = 0.1016 cm; p_L = 0.917 atm (92.9 kN/m^2).

(d) d_0 = 0.2032 cm; p_L = 0.676 atm (68.5 kN/m^2).

L-72-2420

Figure 14.- Spray photographs for mean drop-size measurement, showing position of scattering-light beam in cyanogen-oxygen facility. T_L = 292 K.

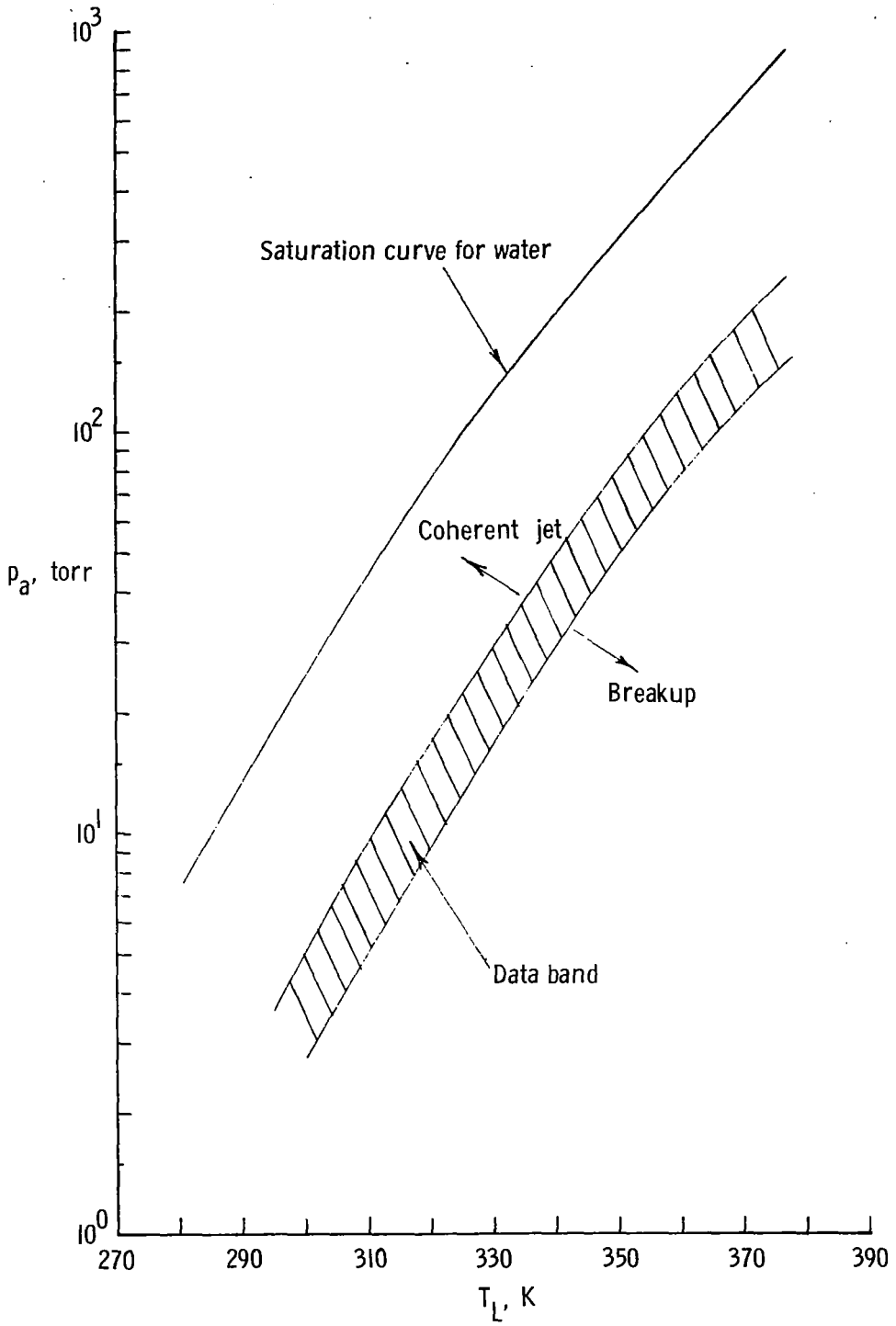

(a) d_o = 0.0254 cm and 0.058 cm; standard orifices (ref. 3).

Figure 15.- Variation of vapor-pressure breakup shattering temperature with ambient pressure in static environment (bell jar) apparatus.

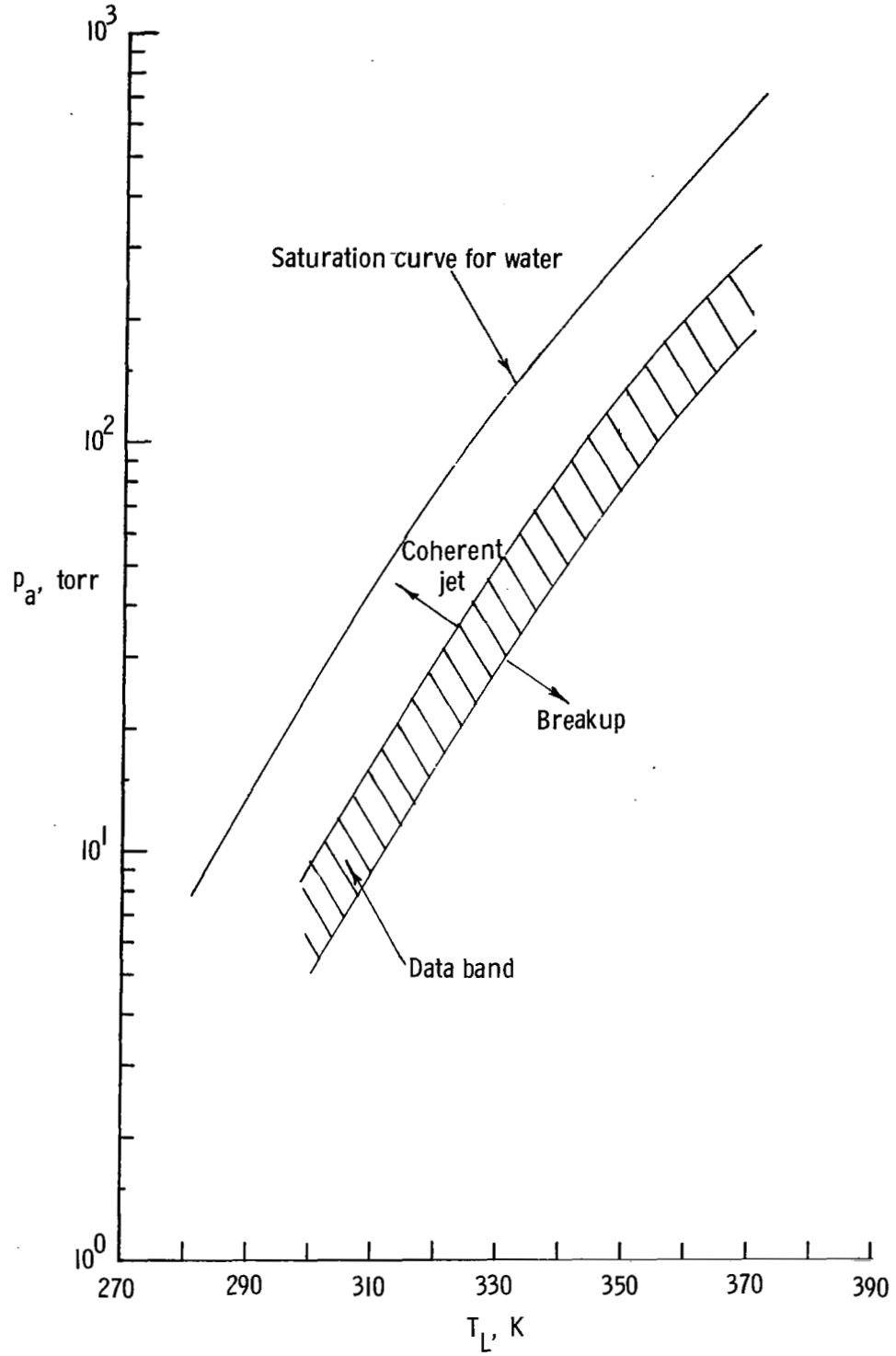

(b) d_o = 0.076 cm and 0.101 cm; standard orifices (ref. 3).

Figure 15.- Continued.

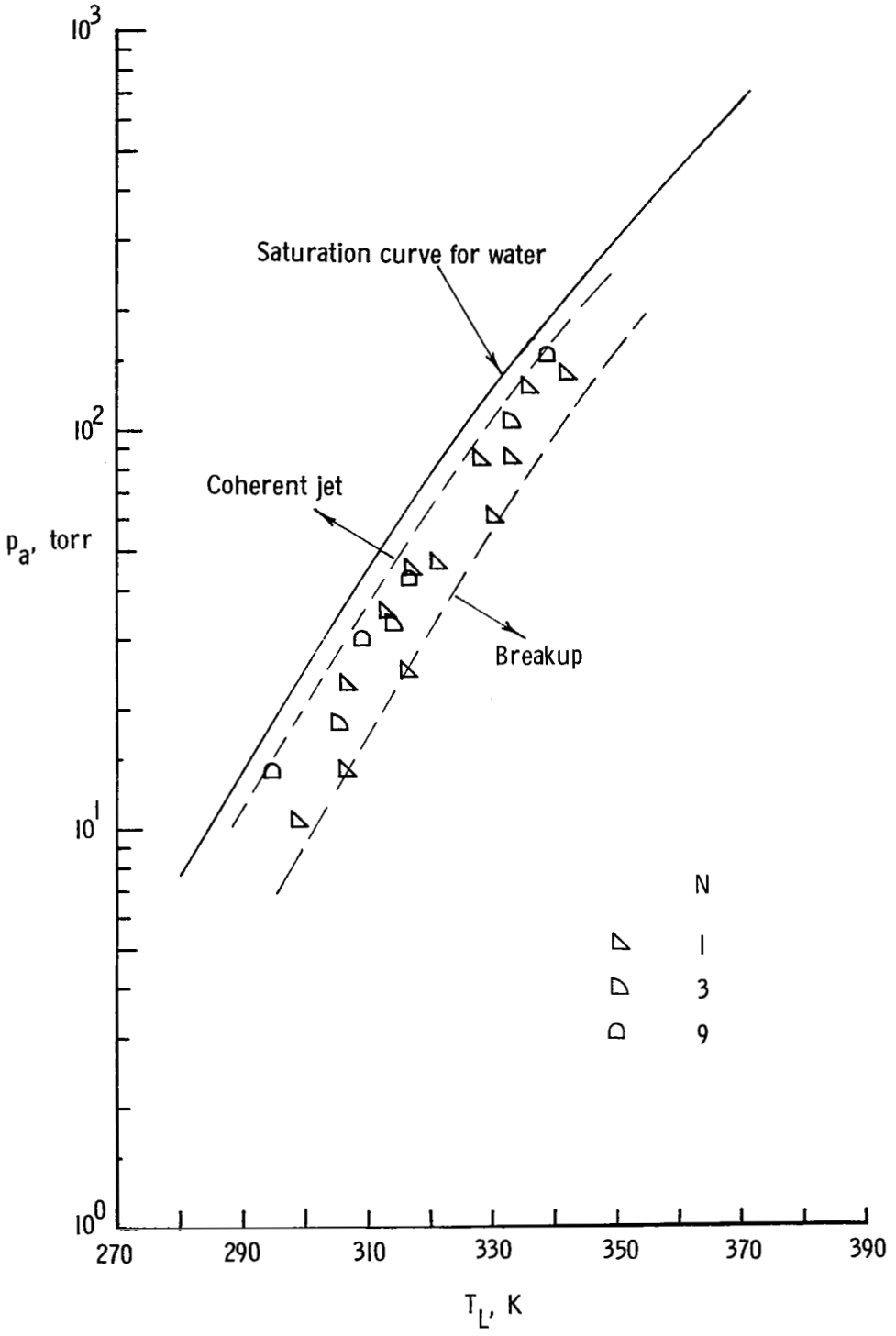

(c) d_o = 0.0457 cm; RAM C-I configuration.

Figure 15.- Concluded.

The data for the RAM C-I type nozzles (see fig. 15(c)) indicate even smaller values of superheat to shatter the jet (5 to 10 K). This may be reasonable in view of the discussion of figures 15(a) and 15(b), as the RAM nozzles have a long L/d_o (RAM C-I = 10; RAM C-III = 5) and an abrupt entrance region all of which should promote nucleation and two-phase flow within the nozzles.

Aerodynamic environment.- Much of the results of the investigation in a Mach 5.5 cyanogen-oxygen tunnel of the aerodynamic breakup boundary (critical Weber number) has been previously reported in reference 8. Figure 5 shows the sprays (T_L = 4.4° to 7.8° C) from four standard research orifices of 0.2032, 0.1016, 0.0508, and 0.0254 cm in diameter representing successively decreasing Weber numbers from 31.4 to 3.9. Varying the orifice diameter was the only available method for changing Weber number $\left(\rho_g V_g^2 d_o/2\sigma\right)$. It can be seen from the photographs that the breakup process is an increasing function of jet diameter. The critical orifice diameter, which is the orifice diameter associated with the critical Weber number, is judged from the photographs to be approximately 0.04 cm, with $We_{,crit} \approx 6$ for the Knudsen numbers of these tests which were of the order 1.0. This data point provides confidence in the use of the critical Weber number concept in the determination of the aerodynamic breakup boundary at near free-molecular conditions.

Previous data from the literature provide a nearly identical value of critical Weber number $\left(We_{,crit} \approx 6\right)$ for continuum conditions $\left(K_n \approx 10^{-5}\right)$. To investigate the variation, if any, of $We_{,crit}$ between $K_n = 10^{-5}$ and 1.0 additional tests were performed in the high Mach number test section (M = 4.5) of the Langley Unitary Plan wind tunnel where low Weber number breakup data were obtained from four standard research orifices with diameters of 0.0127, 0.0254, 0.0508, and 0.1016 cm. Typical scattered-light photographs corresponding to the lowest Weber number conditions are shown in figure 16. A summary of the experimental conditions of the UPWT tests is presented in table I.

It was unfortunate that the UPWT could not be operated at lower dynamic pressures without flow breakdown because it is evident from figure 16 that the spray at $We = 7.6$ is quite close to the critical condition. However, even though these data do not extend into the no-breakup region, the present authors feel certain that the $We_{,crit}$ for $K_n = 10^{-2}$ is reasonably close to that value $\left(We_{,crit} = 6.0\right)$ determined for $K_n = 1.0$ and 10^{-5} and that no appreciable effect of Knudsen number or high local static temperature on critical Weber number seems to exist for primary aerodynamic atomization of liquid jets injected perpendicularly into a gaseous cross flow.

Determination of Drop Size

Static environment.- The data resulting from an investigation of mean drop size for flashing jets from standard research-type orifices in a static environment (bell jar) have

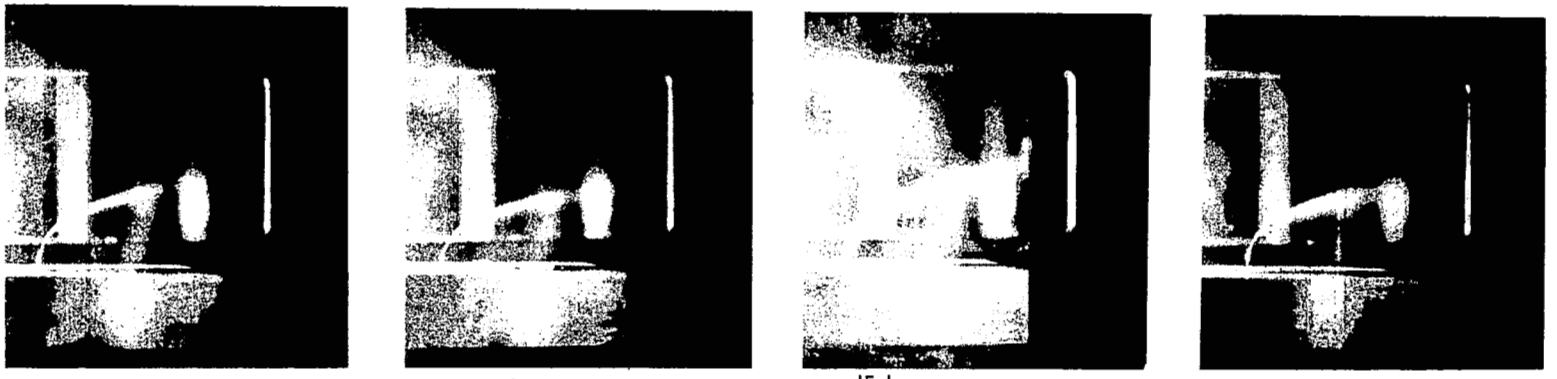

L-72-2421

Figure 16.- Spray photographs from tests in the Unitary Plan wind tunnel. Lowest Weber number sprays from four different orifices; M = 4.5.

TABLE I.- UPWT EXPERIMENTAL CONDITIONS

[$M = 4.5$; $p_L = 1$ atm $(10^5$ N/m$^2)$; $T_t = 339$ K]

Run number	Tunnel stagnation pressure, atm (a)	d_o, cm	Tunnel static pressure, torr (b)	T_L, °C	R	K_n	W_e	$\frac{\rho_L V_L^2}{\rho_g V_g^2}$
1	3	0.1016	8.7	7.8	1200	0.068×10^{-2}	242	2.39
2	↓	.0127	8.7	8.9	↓	.54	30	↓
3		.0254	8.7	8.3		.27	60	
4		.0508	8.8	10.0		.14	121	
5	2	0.1016	5.8	14.4	800	0.10×10^{-2}	162	2.93
6	↓	.0127	5.8	8.3	↓	.82	20	↓
7		.0254	5.7	9.4		.41	40	
8		.0508	5.8	10.6		.20	81	
9	1	0.1016	2.8	13.3	400	0.21×10^{-2}	80	4.18
10	↓	.0127	2.8	6.7	↓	1.66	10	↓
11		.0254	2.8	8.9		.83	20	
12		.0508	2.8	10.6		.42	40	
13	0.816	0.0127	2.1	4.4	300	2.22×10^{-2}	7.6	4.78
14	↓	.0254	2.1	8.3	↓	1.11	15	↓
15		.0508	2.1	9.4		.55	30	
16		.1016	2.1	10.6		.28	61	

[a] 1 atm = 10^5 N/m^2.

[b] 1 torr = 133 N/m^2.

been previously reported in reference 7. Figure 17 presents a summary of these data in the form of a normalized mean diameter versus spray temperature. Also shown in figure 17 are the drop sizes resulting from single orifice RAM C-I type nozzles (0.0457 cm in diameter). Injection pressure was varied from 0.27 to 1.96 MN/m^2, ambient pressures from 3.5 to 103 torr (0.47 to 13.7 kN/m^2) and spray temperatures from 295 to 400 K. In each case, the spray was heated to a temperature greater than the value necessary for jet disintegration, as determined for these nozzles in the previous section for the ambient pressures of these tests. Measurements were made on the center line of the spray nozzles at $y \approx 12$ cm. The main conclusion to be drawn from figure 17 is that the spray from the RAM type nozzles appears to be similar to that from the standard nozzles (ref. 7) in that, under low Weber number conditions, the resultant mean drop size depends primarily on the temperature of the injected water and the orifice diameter.

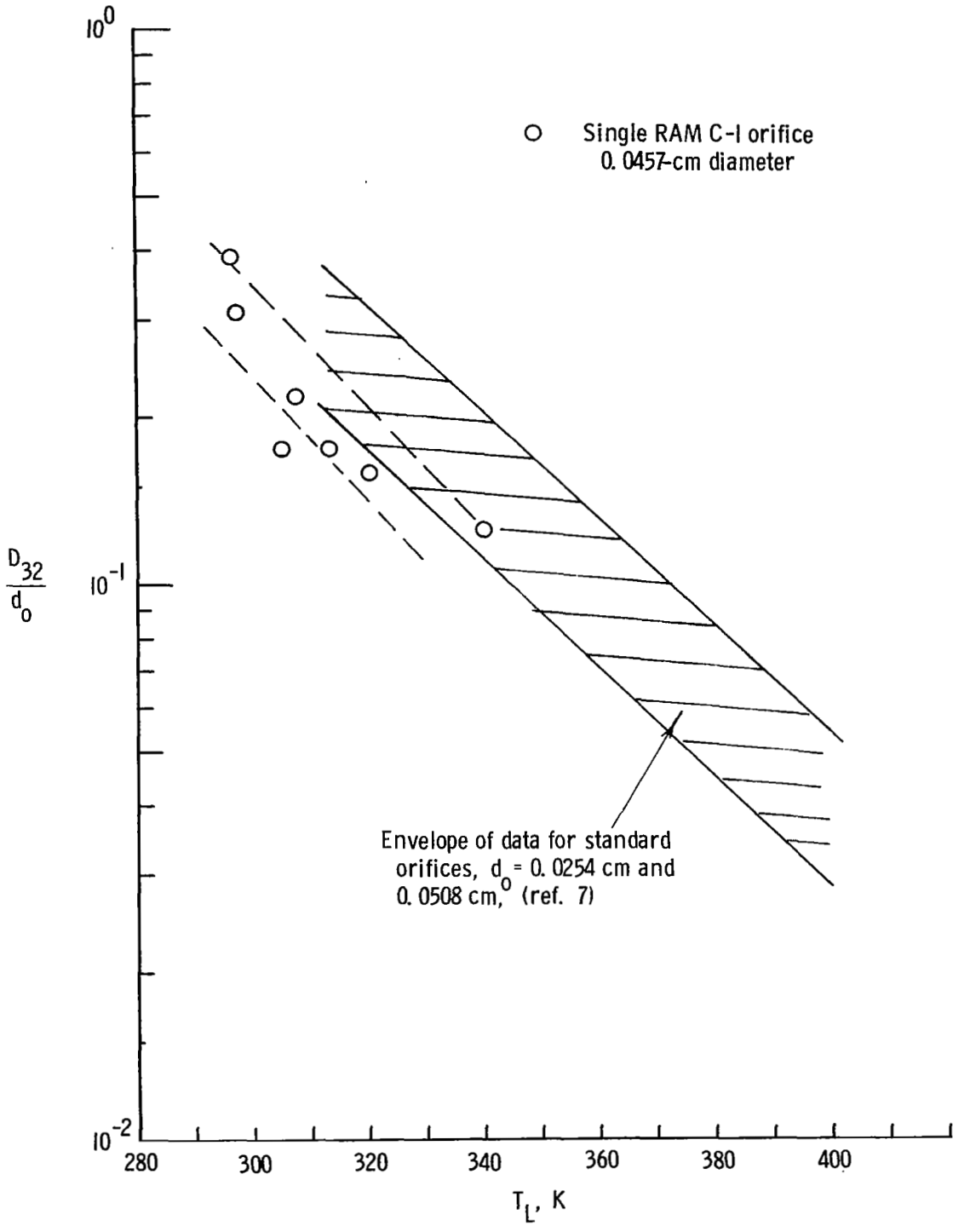

Figure 17.- Variation of normalized mean drop size with spray temperature. y = 12 cm; static environment (bell jar) apparatus.

Physical differences between the standard orifices and the RAM C type nozzles might be expected to give slightly different drop sizes because of the expected increased number of nucleation sites within the spray water in the nozzle exit plane for the RAM nozzle (due to the longer L/d_o). This expectation is borne out in figure 17 by the somewhat smaller mean drop size exhibited by the RAM results compared to those for the standard orifices from reference 7.

Aerodynamic environment.- The results of the drop-size measurements in the Mach 8 wind tunnel have been previously reported in reference 17. New drop-size data, resulting from the investigation in a Mach 5.5 cyanogen-oxygen tunnel, were obtained for normal injection from standard research orifices for two different spray temperatures, $T_L = 19^o$ and 2^o C. The 2^o C injection tests minimize vapor-pressure effects. By injection at these particular temperatures, therefore, mean drop size at approximately the injectant temperatures of the RAM C-I and C-III flights ($T_L \approx 24^o$ and 19^o C) can be obtained, and in addition, mean drop size with and without vapor-pressure breakup can also be determined.

Figure 18 shows the mean drop-size data D_{30}/d_o plotted as a function of $W_L{}^{3/2}(R/M)$. In addition, the drop-size data for the Mach 8 and cyanogen-oxygen tunnel tests are tabulated in tables II and III. The D_{32} were found to be independent of V_{H_2O} over the test range, which was $25 \text{ m/s} \leqq V_{H_2O} \leqq 82 \text{ m/s}$. This is in agreement with the correlations of references 12 and 13. The data have been plotted as suggested by reference 16, according to a modified Volynskiy (ref. 13) correlation. The measured D_{32} has been converted to D_{30}, using the Nakiyama-Tanasawa size distribution expression, as follows (ref. 12):

$$D_{30} = 0.783 D_{32}$$

Also shown is the modified Volynskiy correlation expression from reference 16:

$$\frac{D_{30}}{d_o} = \frac{48}{\left[W_L{}^{3/8}(R/M)^{1/4}\right]}$$

which is plotted as a solid line.

The cyanogen-oxygen data are seen to be unaffected by liquid temperature. (The 19^o C data agree with the 2^o C data.) This indicates that the aerodynamic breakup mechanism, when present ($W_e > W_{e,crit}$), seems to override the vapor-pressure breakup mechanism ($T_L > T_s$). The cold injectant temperatures correspond to $T_L < T_s$ and thus the aerodynamic effect is the only breakup mechanism available for these data. Therefore, during flight, once $W_e > W_{e,crit}$, the drop size would be expected to decrease to the aerodynamic value even though $T_L > T_s$ (see fig. 15(c)).

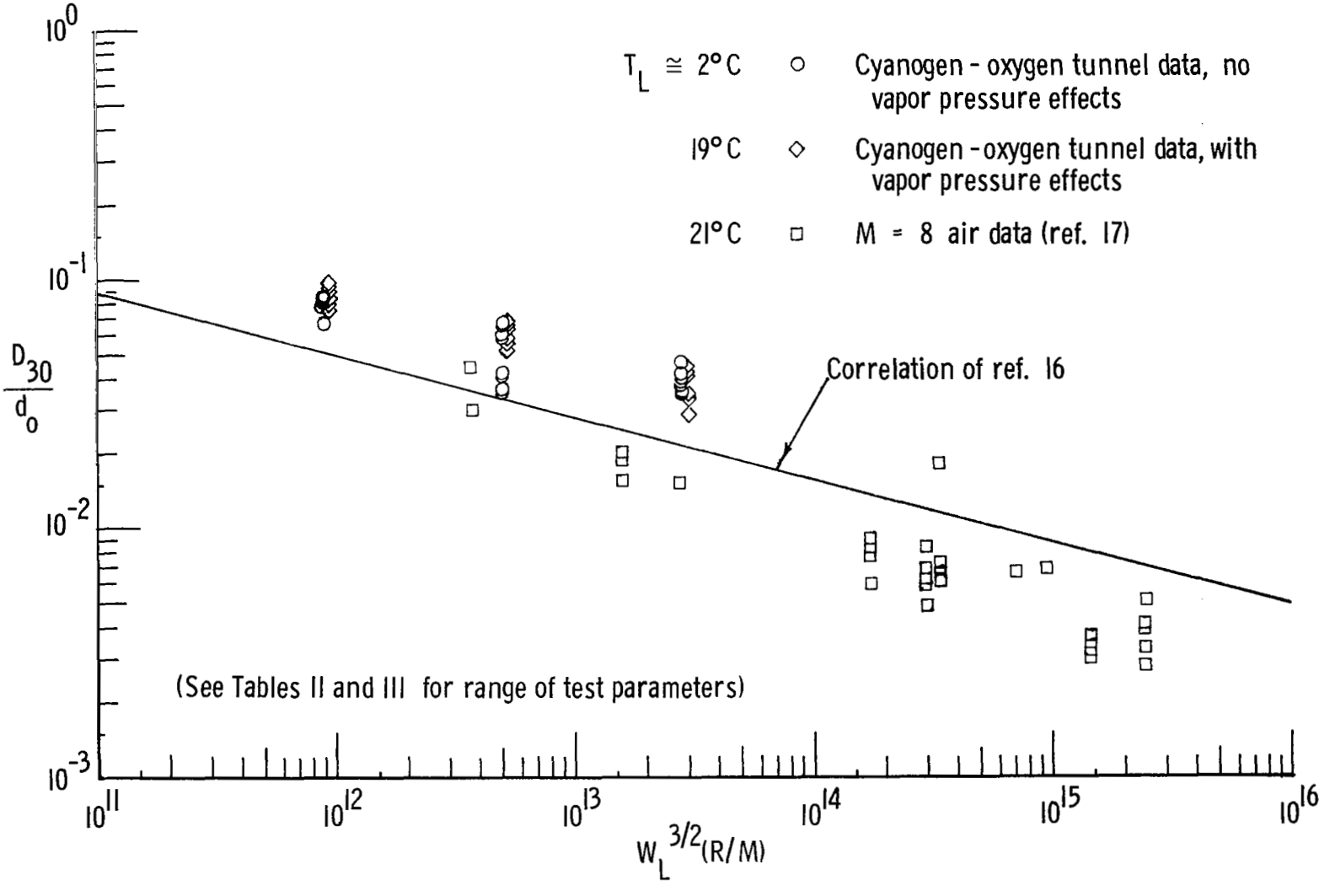

Figure 18.- Comparison of mean drop-size data with previous results (ref. 5), aerodynamic breakup.

TABLE II.- DROP-SIZE DATA FROM MACH 8 TUNNEL

$[T_L = 21^{\circ}$ C; M = 7.95]

Run number	d_o, cm	T_t, K	p_t, atm (a)	p_a, torr (b)	W_e	W_L	R	$W_L^{3/2}(R/M)$	D_{32}, μm	D_{30}/d_o
5526	0.1321	777	35	2.84	320	2.64×10^7	1.03×10^4	1.77×10^{14}	-----	----------
27	↓	↓	↓	↓	↓	↓	↓	↓	13	7.7×10^{-3}
28									13	7.7
29									15	8.9
30									13	7.7
31									10	5.9
32									15	8.9
34		797	63.6	5.16	564		1.79×10^{14}	3.06×10^{14}	12, 14	7.1, 8.3
36		766	35	2.84	317		1.03×10^4	1.77×10^{14}	15	8.9
37		↓	↓	↓	↓		↓	↓	14	8.3
38									15	8.9
39									12	7.1
40									12	7.1
41		739	7.8	.634	72		2.48×10^3	4.24×10^{13}	19	1.1×10^{-2}
42			8.5	.690					20	1.2
44									20	1.2
46									18	1.1
47		805	62.2	5.05	570		1.79×10^4	3.06×10^{14}	-----	----------
48									13	7.7×10^{-3}
49									11	6.5
50									8, 11	4.8, 6.5
51	↓	↓	↓	↓	↓	↓	↓	↓	10	5.9
52	.0508	766	35	2.84	120	1.02×10^7	3.97×10^3	1.63×10^{13}	10	1.5×10^{-2}
54		↓	↓	↓	↓		↓	↓	11.5	1.8
55									13	2.0
58		744	7.4	.683	28		9.53×10^2	3.91×10^{12}	28	4.3
59		750	7.4	.678	28		9.53×10^2	3.91×10^{12}	19	2.9
60	↓	808	62.2	5.05	220	↓	6.88×10^3	2.82×10^{13}	10	1.5
67	.3048	777	35	2.84	730	6.1×10^7	2.38×10^4	1.43×10^{15}	12.5	3.2×10^{-3}
68		↓	↓	↓	↓		↓	↓	12	3.1
69									14	3.6
70									14.5	3.7
71									14	3.6
72		797	62.5	5.07	1300		4.13×10^4	2.48×10^{15}	11	2.8
73		↓	62.2	5.05	↓		↓	↓	16	4.1
74			62.2	5.05					13	3.3
75		741	8.1	.66	168		5.72×10^3	3.43×10^{14}	28	7.2
76		↓	8.5	.69	↓		↓	↓	28	7.2
77			8.3	.67					24, 27	6.2, 6.9
78			8.3	.67					70	1.8×10^{-2}
80		775	14.6	1.19	360		1.18×10^4	7.05×10^{14}	26	6.7×10^{-3}
81		792	25.5	2.07	498		1.59×10^4	9.52×10^{14}	27	6.9
82	↓	816	62.9	5.10	1334	↓	4.13×10^4	2.48×10^{15}	15, 20	3.8, 5.1

[a] 1 atm = 10^5 N/m^2.

[b] 1 torr = 133 N/m^2.

TABLE III.- DROP-SIZE DATA FROM CYANOGEN-OXYGEN TUNNEL

[T_t = 4500 K; p_t = 1 atm (10^5 N/m^2); p_a = 0.48 torr (64 N/m^2); M = 5.5]

Run number	d_o, cm	T_L, °C	We	W_L	R	$W_L^{3/2}(R/M)$	D_{32}, μm	D_{30}/d_o
25-1	0.2032	16.7	32.0	2.49×10^8	41.8	3.01×10^{13}	90	3.5×10^{-2}
2	↓	↓	↓	↓	↓	↓	74	2.9
3	↓	↓	↓	↓	↓	↓	88	3.4
4	.1016	↓	16.0	1.24×10^8	20.9	5.32×10^{12}	70	5.4
5	↓	↓	↓	↓	↓	↓	75	5.8
6	↓	↓	↓	↓	↓	↓	66	5.1
7	.0508	↓	8.0	$.62 \times 10^8$	10.5	$.94 \times 10^{12}$	48	7.4
8	↓	↓	↓	↓	↓	↓	44	6.8
9	↓	↓	↓	↓	↓	↓	50	7.7
26-1	.2032	18.9	32.0	2.49×10^8	41.8	3.01×10^{13}	110	4.2
2	↓	↓	↓	↓	↓	↓	108	4.2
3	↓	↓	↓	↓	↓	↓	115	4.4
4	.1016	↓	16.0	1.24×10^8	20.9	5.32×10^{12}	84	6.5
5	↓	↓	↓	↓	↓	↓	82	6.3
6	↓	↓	↓	↓	↓	↓	86	6.6
7	.0508	↓	8.0	$.62 \times 10^8$	10.5	$.94 \times 10^{12}$	58	8.9
8	↓	↓	↓	↓	↓	↓	64	9.9
9	↓	↓	↓	↓	↓	↓	64	9.6
27-1	.2032	2.8	31.0	2.40×10^8	41.8	2.85×10^{13}	104	4.0
2	↓	↓	↓	↓	↓	↓	108	4.2
3a	↓	↓	↓	↓	↓	↓	98	3.8
3b	↓	↓	↓	↓	↓	↓	99	3.8
4	↓	↓	↓	↓	↓	↓	107	4.1
5b	↓	↓	↓	↓	↓	↓	108	4.1
5a	.1016	3.9	15.5	1.20×10^8	20.9	5.04×10^{12}	54	4.1
6	↓	↓	↓	↓	↓	↓	46	3.6
7	↓	↓	↓	↓	↓	↓	45	3.5
8	↓	↓	↓	↓	↓	↓	54	4.2
28-1	↓	1.7	↓	↓	↓	↓	75	5.8
2	↓	↓	↓	↓	↓	↓	84	6.5
3	↓	↓	↓	↓	↓	↓	86	6.6
4	↓	↓	↓	↓	↓	↓	76	5.9
5	.0508	2.8	7.8	$.60 \times 10^8$	10.5	$.89 \times 10^{12}$	43	6.6
6	↓	↓	↓	↓	↓	↓	54	8.3
7	↓	↓	↓	↓	↓	↓	52	8.0
8	↓	↓	↓	↓	↓	↓	55	8.5
9	.2032	1.7	31.0	2.4×10^8	41.8	2.85×10^{13}	120	4.6
10	↓	↓	↓	↓	↓	↓	95	3.7
11	↓	↓	↓	↓	↓	↓	94	3.6
12a	↓	↓	↓	↓	↓	↓	90	3.5
12b	↓	↓	↓	↓	↓	↓	93	3.6

Also of interest in figure 18 is the fact that the cyanogen-oxygen tunnel data at low W_e are above the reference 16 correlation whereas the Mach 8 data at larger W_e are generally below. Although the possibility of a systematic error between the data obtained in the Mach 8 tunnel and that obtained in the Mach 5.5 cyanogen-oxygen tunnel cannot be ruled out, the actual data used in reference 16 to obtain the correlation shown are in agreement with the trends of the present results (above the correlation at low W_e and below it at high W_e). In fact, a "kink" in the data used in reference 16 appears to be present at $W_L{}^{3/2}(R/M) \approx 10^{13}$. There is a possibility that this apparent anomaly may be due to a change in the atomization mechanism. Reference 21 suggests that, at comparatively low W_e, the primary droplet-production mechanism is caused by capillary wave action, whereas at higher W_e, acceleration waves cause droplet production and presumably smaller drops. The dividing line seems to be in the vicinity of $W_e = 50$ (ref. 21 and table II). It would therefore seem that a single drop-size correlation may not be applicable over the entire range of interest for liquid injection into an airstream. Reference 22 provides first-order estimates for the mean drop sizes produced by the two breakup modes discussed in reference 21.

Penetration

Several methods and data correlations are currently available to compute spray penetration for high Weber number conditions (refs. 23 to 29). To determine the effect of low Weber number (low-dynamic-pressure) conditions upon maximum spray penetration, the present penetration data are shown compared with the previous high Weber number results in figure 19. The data are shown for $x/d_o = 100$. The present Mach 8 results, which correspond to a fairly high Weber number situation, are in reasonable agreement with the prediction of reference 23. However, the present UPWT and cyanogen-oxygen-facility data are considerably above these higher Weber number results (almost a factor of two increase) and, also, the present data exhibit a consistent variation with d_o in disagreement with the previous results (refs. 23 to 25).

A possible reason for these higher penetration values is the same mechanism mentioned in connection with figure 18; that is, the possibility, as advocated in references 21 and 22, of a different breakup mechanism at low dynamic pressure (capillary waves) than at high dynamic pressure (acceleration waves). Also, as mentioned previously, when the Weber number is reduced sufficiently, conventional aerodynamic breakup no longer occurs (y_{max}/d_o becomes large) and therefore, as the Weber number is increased from such a low value, one might expect the y_{max}/d_o values to approach the previous large dynamic pressure results from the high side. In any event, figure 19 indicates that methods such as advocated in reference 23 evidently cannot yield accurate predictions for high-altitude (low-dynamic-pressure) conditions. The streamwise variation of maximum

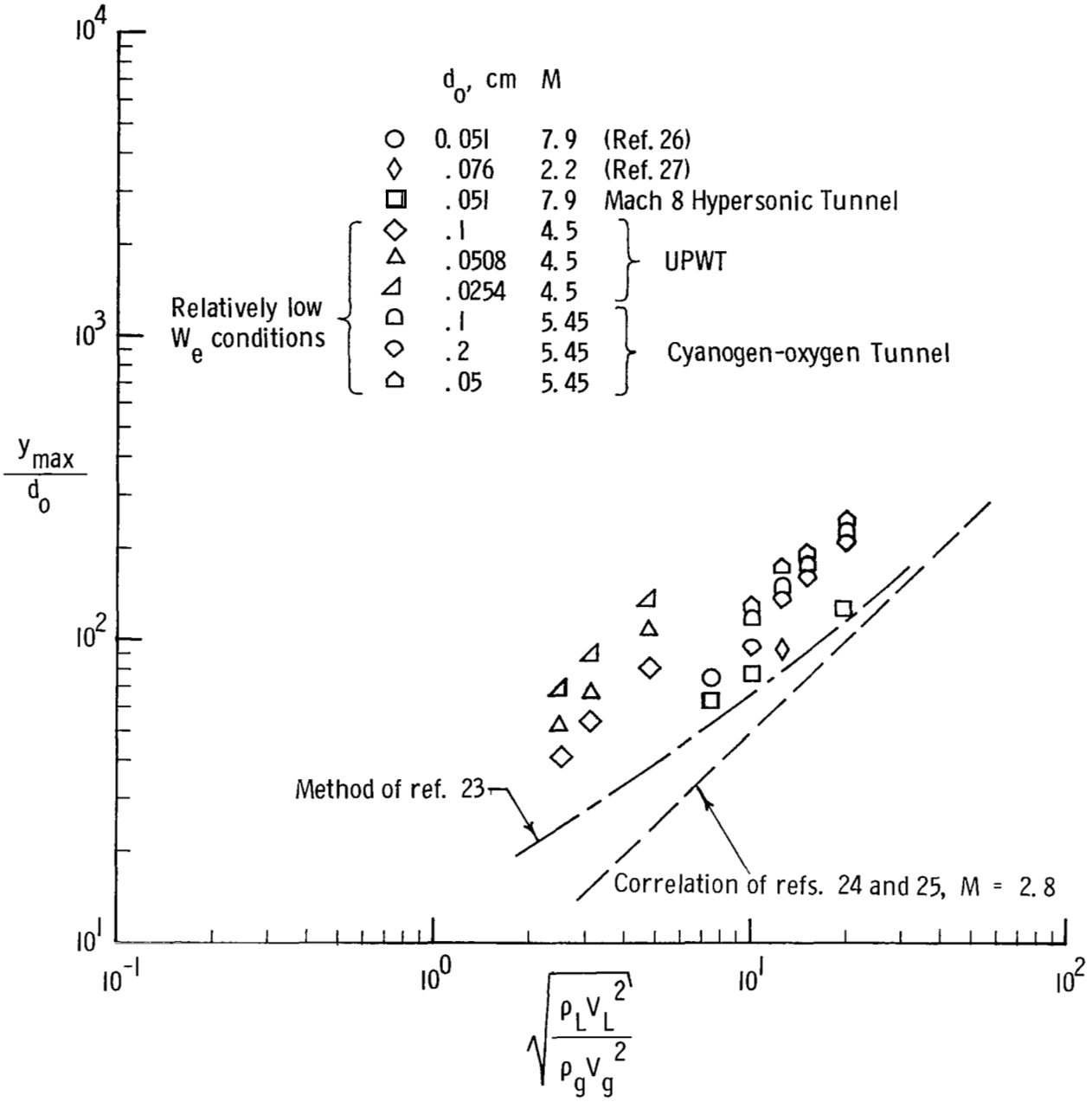

Figure 19.- Comparison of present penetration data at low Weber number conditions with previous high Weber number results. $x/d_o = 100$; $d_e/d_o = 1$; single orifice injection.

penetration is indicated in figure 20 for the present data. The Mach 8 and UPWT results indicate a variation of the form $y_{max}/d_o \propto (x/d_o)^{0.33}$. The present cyanogen-oxygen data indicate a somewhat stronger variation $(y_{max}/d_o \propto (x/d_o)^{0.5})$.

The higher power exhibited by the cyanogen-oxygen results may be due to the conical flow present at the injection site. This would presumably cause a more rapid dispersion of the spray. The present data are in reasonable agreement with previous results (ref. 24) which have indicated variation of the form $y_{max}/d_o \propto (x/d_o)^{0.4}$.

APPLICATION OF RESULTS TO RAM C-I AND C-III FLIGHTS

The RAM C-I and C-III flights were orbital-velocity reentry experiments in which water was injected intermittently from a sphere-cone (9^o half-angle) in the sphere-cone juncture region. The experiments are described in considerable detail in references 1 and 30 along with the blackout-alleviation effects of the injection. In this section we will apply the results of our ground research to determine the various water breakup boundaries during the flight and recommend appropriate expressions for resultant drop size when breakup does occur. The maximum velocity for the C-I flight was 7670 m/s at 74.7 and 67 km, and for the C-III flight was 7408 m/s at 71.6 km.

The multiple orifice nozzles employed in the RAM C-I flight (injection angle, 90^o to the cone surface) have been sketched in figure 1. The nozzles for the C-III flight are of similar design, but slightly larger, with an outside diameter of 0.508 cm, $d_o = 0.0508$ cm, an overall length of 1.46 cm, $L/d_o = 10$, and $N = 1, 3, 5$, and 7. The injection angle of C-III is 51^o. The nozzles actually tested for the investigations reported herein were of the C-I design and only injection angles of 90^o were used. However, difficulty in application of the ground-research results to the C-III flight conditions is not expected, provided that the local dynamic pressure calculated for oblique injection are reduced by a factor equal to $(\cos \alpha)^2$ (i.e., the effective velocity and Mach number tending to cause breakup of the water jet is presumably that component perpendicular to the jet). Additionally, the flight nozzles were mounted in clusters (ref. 30). These various arrangements were not simulated in the present tests since clusters of multiple orifice nozzles would have produced a mist too dense to be satisfactorily analyzed by the scattered-light technique.

Considering first the possibility of vapor-pressure breakup, the local pressure level at the water injection site is shown in figure 21 as a function of altitude. The pressure levels are shown for several streamlines and were obtained from calculations performed in reference 31. The calculation procedure (ref. 31) includes effects of nonequilibrium chemistry on the local flow properties and the results are probably accurate except at high altitudes (above ≈65 km) where viscous effects become large. For water injected at

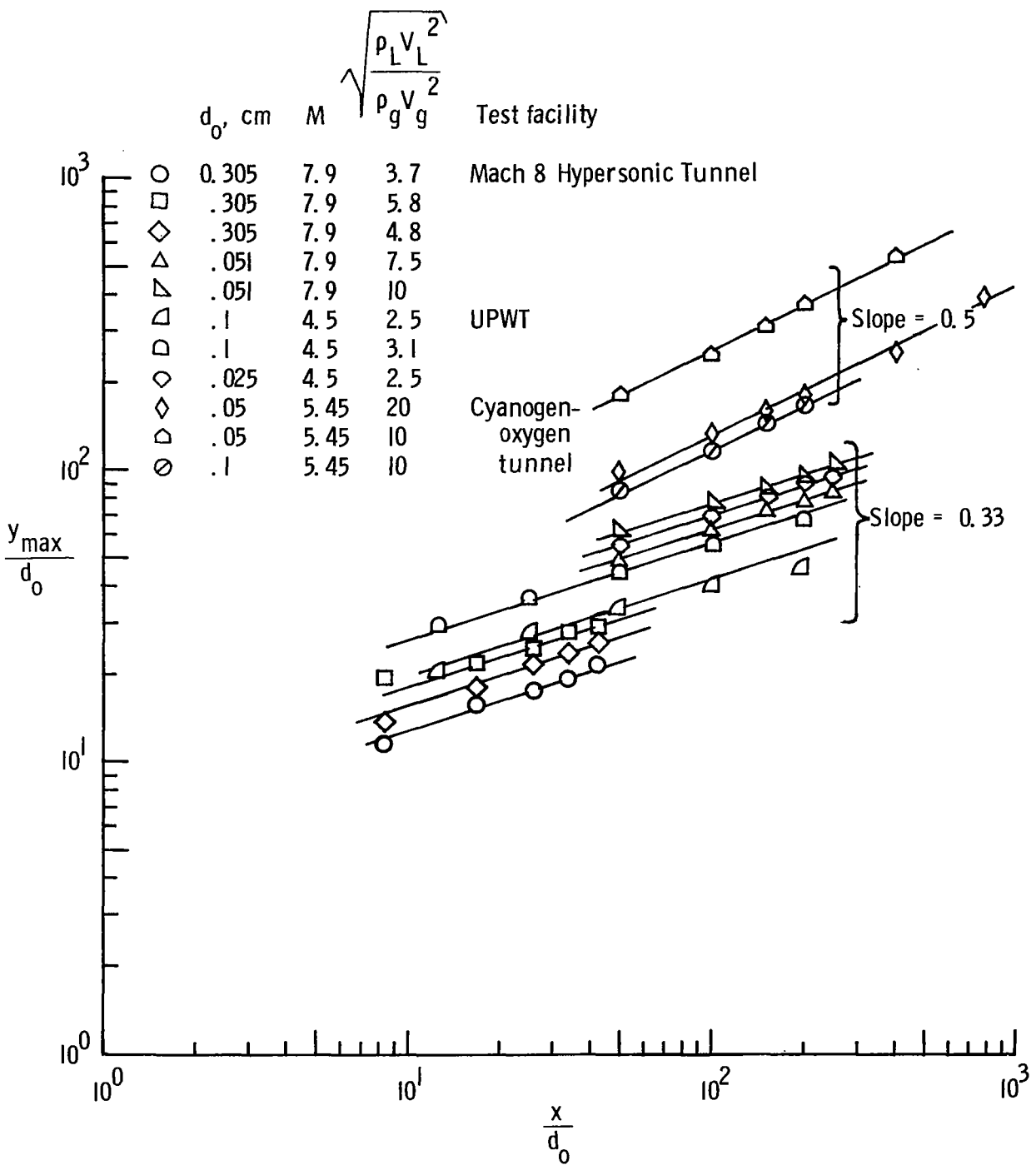

Figure 20.- Variation of outermost penetration in streamwise direction. Single orifice injection.

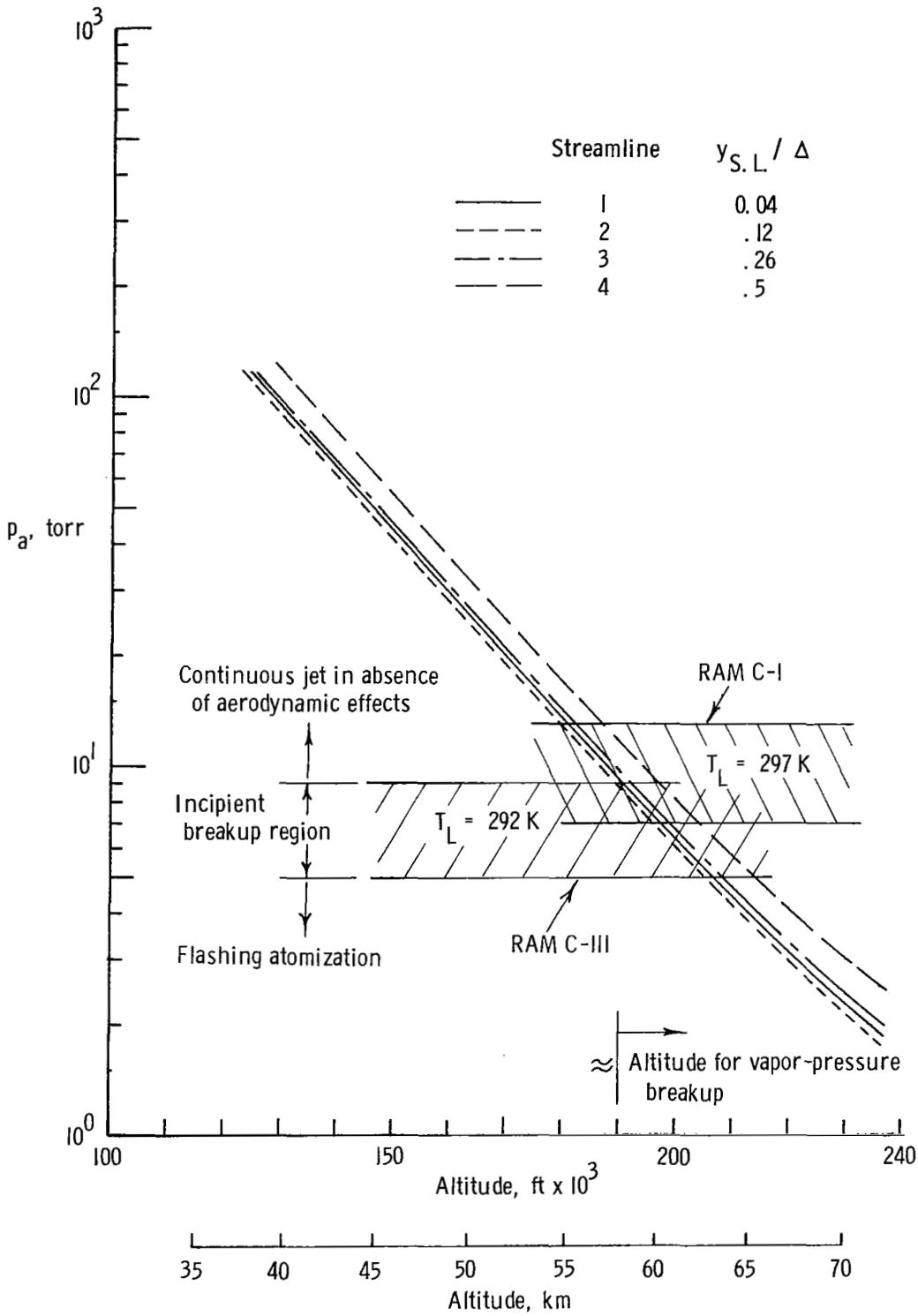

Figure 21.- Breakup boundary for vapor-pressure atomization of RAM C-I and C-III flights. d_o = 0.0457 cm; injection station (x/D = 0.54).

297 K (the most probable water temperature during the C-I flight) figure 15(c) for the C-I orifices yields a breakup region between approximately 7 and 13 torr (933 and 1733 N/m^2). As indicated in figure 21, this breakup region indicates that vapor-pressure breakup probably occurred for altitudes greater than approximately 57 km. The estimated water temperature for the C-III flight (292 K) gives a breakup region between 5 and 9 torr (666 and 1200 N/m^2); and hence vapor-pressure breakup probably occurred for altitudes greater than approximately 61 km.

The cyanogen-oxygen-tunnel data shown in figure 18 indicated that, if aerodynamic breakup occurs, the resultant drop size is essentially that for aerodynamic breakup even though vapor-pressure breakup may be occurring simultaneously with the aerodynamic mechanism. Therefore, the breakup boundary for aerodynamic atomization is investigated in figure 22.

The local Weber number is shown as a function of altitude for the same streamlines considered in figure 21. Again the local properties were obtained from calculations performed in reference 31. From reference 8 and the UPWT tests described herein, the breakup criterion for aerodynamic atomization, even for the high K_n flight conditions (Altitude > 60 km), is a value of W_e from 4 to 6. This breakup boundary is indicated in figure 22. Comparison of the local W_e values with the breakup boundary indicates that for altitudes less than approximately 75 km there is a good probability that aerodynamic breakup occurred. This result, combined with previous statements concerning the cyanogen-oxygen-tunnel droplet measurements with warm and cold water (where the aerodynamic breakup mechanism, when present, overrode vapor-pressure effects), indicates that below 75 km the RAM C water-injection data can be analyzed using the aerodynamic drop-size correlations shown in figure 18.

It should be noted that the discussion of the present penetration data for low Weber number $(W_e \lesssim 50)$ conditions indicated higher penetration values than would be predicted by the high Weber number theory and data correlations of references 22 and 23. Therefore, even though aerodynamic atomization evidently occurred for altitudes below approximately 75 km, the penetration down to 55 to 60 km may have been greater than one would expect from using the results of references 23 and 24 due to the fairly low Weber number conditions in this high-altitude region.

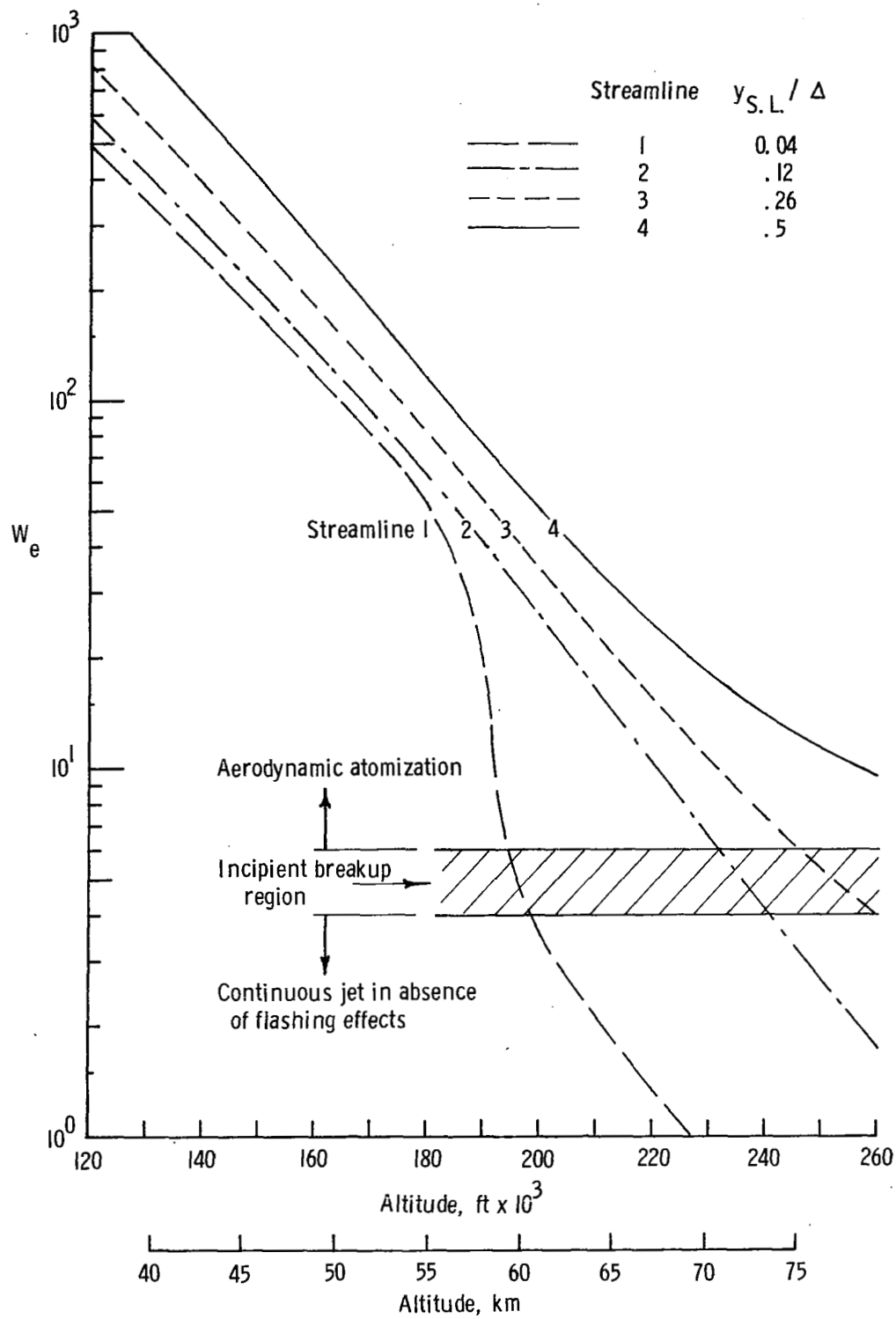

Figure 22.- Breakup boundary for aerodynamic atomization of RAM C flights. d_o = 0.0457 and 0.0508 cm; injection station (x/D = 0.54).

CONCLUSIONS

An experimental program was conducted to determine breakup or atomization boundaries, resultant mean drop sizes, and penetration for water jets at high-altitude reentry conditions. These experiments were carried out in a static environment (bell jar), in conventional aerodynamic wind tunnels at Mach numbers of 4.5 and 8, and in a high-temperature, low-density Mach 5.5 cyanogen-oxygen combustion tunnel. The following conclusions can be drawn:

1. Incipient vapor-pressure breakup in the absence of external flow can occur at superheats from 5 to 25 K, depending upon the orifice configuration.

2. The resultant mean drop size for vapor-pressure breakup, in the absence of external flow, is directly proportional to the orifice diameter and is an inverse function of the absolute temperature of the injectant.

3. A breakup boundary for aerodynamic atomization occurs at a Weber number of approximately 4 to 6, and is not a function of Knudsen number.

4. The resultant drop sizes observed for aerodynamic atomization at low Weber numbers are 70 to 80 percent above the recent correlation of NASA CR-1242, while those observed at high Weber numbers are 80 to 100 percent below the same correlation.

5. When both aerodynamic and flashing breakup occur, the drop size corresponds to the aerodynamic value (when the aerodynamic value is less than the vapor-pressure drop size).

6. The penetration at low Weber number ($\lesssim 50$) conditions exceeds by up to a factor of two the predictions and data correlation from previous high Weber number ($\gtrsim 500$) studies.

7. Application of the present results to the RAM C trajectories indicates that aerodynamic atomization probably dictated resultant mean drop size for altitudes less than approximately 75 km.

Langley Research Center,
National Aeronautics and Space Administration,
Hampton, Va., May 2, 1972.

APPENDIX

MODIFICATION OF SCATTERED-LIGHT DISTRIBUTION CURVE UPON REPLACEMENT OF POINT SOURCE WITH SLIT SOURCE

The light-scattering technique for measurement of D_{32}, which was reported in reference 18, was selected for use in the experiments described in this report. A slit source was substituted for the point source in order to increase the amount of light passing through the spray and thus to increase the amount of scattered light. The mean theoretical illumination profile for the scattered light from a multidispersion illuminated by a point source (fig. 3 of ref. 18) was used to calculate the appropriate illumination profile on the assumption that the slit image and the surrounding scattered-light pattern are due to the superposition of a large number of point images and their associated scattered-light patterns. The sketches of figure 23 are useful in defining the symbols used herein and in describing the procedure used.

Around each point on the x-axis of the slit image there is a radial distribution of scattered light. This distribution is described by the function $F(r)$, normalized so that $I = 1$ at $r = 0$. This scattered light emanates from a line distribution of scattering centers along a line X at a distance f from the x-axis. The light is received at p' at the center of the slit image horizontally, but located at various heights vertically from p (the center of the slit image). That received at p' due to the scattering pattern about p was scattered through the angle $\theta_c = \tan^{-1}(r_c/f)$. That due to the scattering patterns about other point images q, along the slit image. was scattered through the larger angles $\theta = \tan^{-1}(r/f)$ where $r_c \leq r \leq r_m$ and $r_m = \sqrt{r_c^2 + (s/2)^2}$. The total scattered-light intensity at p' is therefore proportional to $2\int_{\theta_c}^{\theta_m} I(\theta)\, d\theta$, where $\theta_m = \tan^{-1}(r_m/f)$ and $I(\theta)$ is obtained from figure 3 of reference 18.

Let $F(r)$ be the original point scattering $I(\theta)$ of reference 18 ($r = f \tan \theta$), and let $I'(\theta)$ be the desired illumination profile for the center of a slit image (plotted against reduced angle $\bar{\theta}$[1]).

When $y = 0$,

$$F(r) \equiv F(x)$$

and when $y \neq 0$,

$$F(r) = F\left(\sqrt{x^2 + y^2}\right)$$

---

[1] Plotting against the reduced angle $\frac{\pi D_{32}}{\lambda}\theta$ allows the same $I'(\theta)$ distribution to be used for various values of D_{32} and λ.

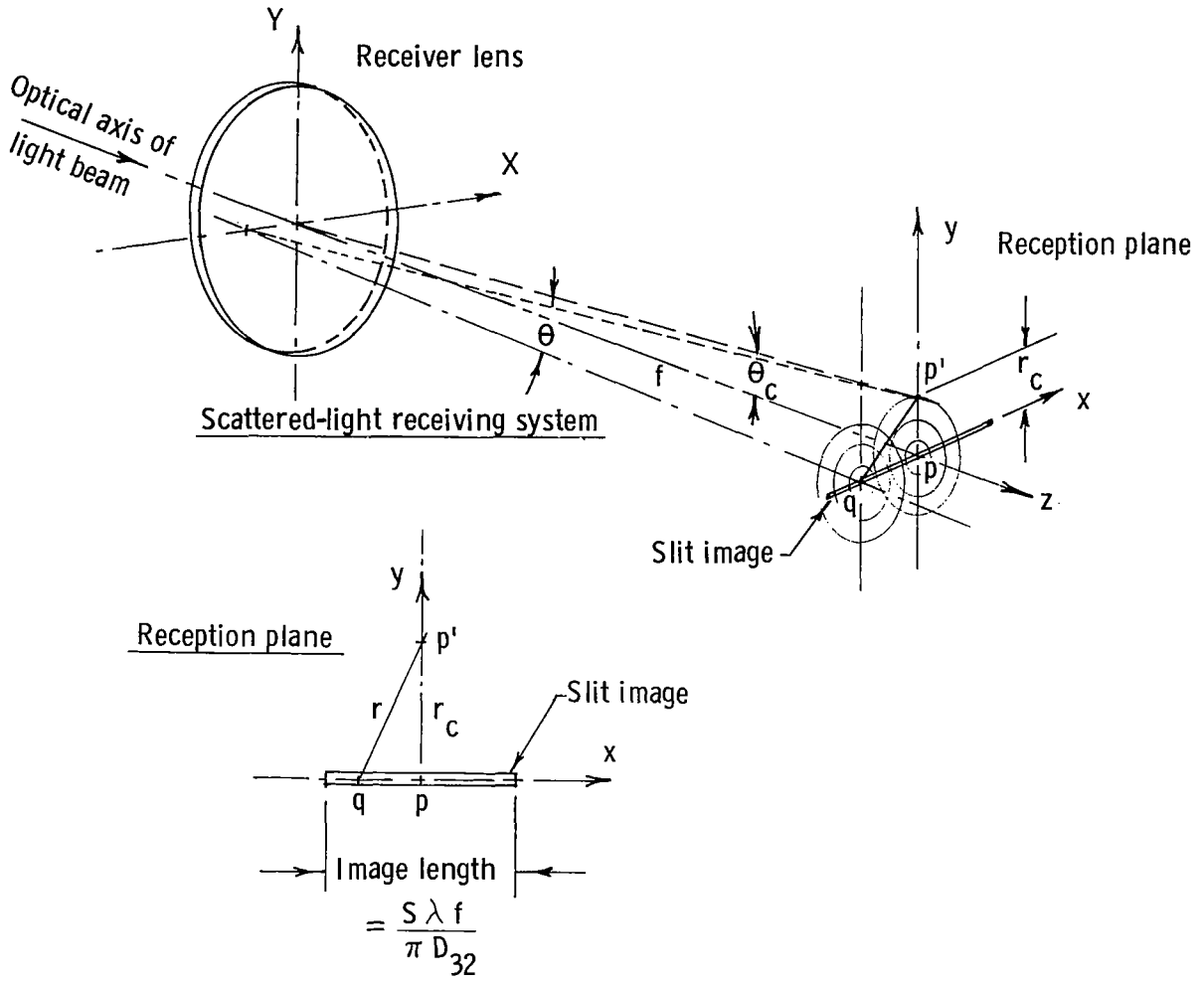

Figure 23.- Geometrical construction for the determination of the diffraction pattern around a slit image.

By curve fitting, it was ascertained that $I(\theta)$ of reference 18 could be approximated by the following series:

$$F(r) = 0.1085e^{-(0.33r)^2} + 0.8915e^{-(0.6425r)^2} + \ldots$$

Therefore,

$$I'(\theta) = \frac{0.1085\sqrt{\pi}}{2(0.33)} \int_a^b \frac{2}{\sqrt{\pi}} e^{-\left[(0.33)^2(x^2+y^2)\right]} (0.33\ dx)$$

$$+ \frac{0.8915\sqrt{\pi}}{2(0.6425)} \int_a^b \frac{2}{\sqrt{\pi}} e^{-\left[(0.6425)^2(x^2+y^2)\right]} (0.6425\ dx)$$

where $a = 0$ and $b = \frac{s}{2} = \frac{S}{2} \frac{f\lambda}{\pi D_{32}}$. Then

$$I'(\theta) = \frac{\sqrt{\pi}}{2}\left\{\frac{0.1085}{0.33} e^{-(0.33y)^2}\left[\operatorname{erf}(0.33b) - \operatorname{erf}(0.33a)\right]\right.$$

$$\left. + \frac{0.8915}{0.6425} e^{-(0.6425y)^2}\left[\operatorname{erf}(0.6425b) - \operatorname{erf}(0.6425a)\right]\right\}$$

Normalization of the $I'(\theta)$ distribution is achieved by dividing all computed values of $I'(\theta)$ by the value of $I'(0)$.

A comparison of the series approximation of $I(\theta)$ with the actual data from reference 18 is shown in figure 24, where it can be seen that the departure of the series distribution from the original data is quite small down to $I(\theta)$ values of 10^{-2} (which is below our measurement capability). However, to determine what effect these small departures of the series approximation would have on the resulting $I'(\theta)$ distribution, the above integration was repeated using the actual $I(\theta)$ of reference 18 with the integration being accomplished by means of a planimeter.

The results of both methods of integration are shown in figure 25 where the $I'(\theta)$ obtained by integrating the series distribution is shown as a series of solid curves. The distribution resulting from the mechanical integration of the $I(\theta)$ from reference 18 is shown as dashed curves. It can be seen from the figure that for practical purposes (down to $I'(\theta)$ values of 10^{-1}) both sets of curves are nearly identical. However, even though the differences were insignificant, in the evaluation of the light-scattering data for this report, where some values of $I'(\theta)$ as low as 5×10^{-2} were encountered, the dashed curves (also tabulated in table IV) are used. Furthermore, there is very little practical difference between $I(\theta)$ and $I'(\theta)$ and in all cases evaluated herein (see fig. 10, for example), it made no difference which distribution, $I(\theta)$ or $I'(\theta)$, was used for comparison.

TABLE IV.- MEAN THEORETICAL ILLUMINATION PROFILES FOR POLYDISPERSIONS FOR VARIOUS SLIT LENGTHS

$\frac{\pi D_{32}\theta}{\lambda}$	$I'(\theta)$ for –				
	S = 0 (a)	S = 0.1	S = 1	S = 4	S = 8, 10, ∞
0.0	1.000	1.000	1.000	1.000	1.000
.4	.925	.927	.940	.942	.943
.8	.778	.780	.795	.800	.801
1.2	.592	.594	.603	.613	.614
1.6	.400	.402	.407	.424	.432
2.0	.233	.234	.239	.262	.274
2.4	.125	.126	.131	.160	.174
3.5	.0328	.0330	.0360	.0564	.062
5.5	.0080	.0083	.0091	.0115	.020

[a] Reference 9.

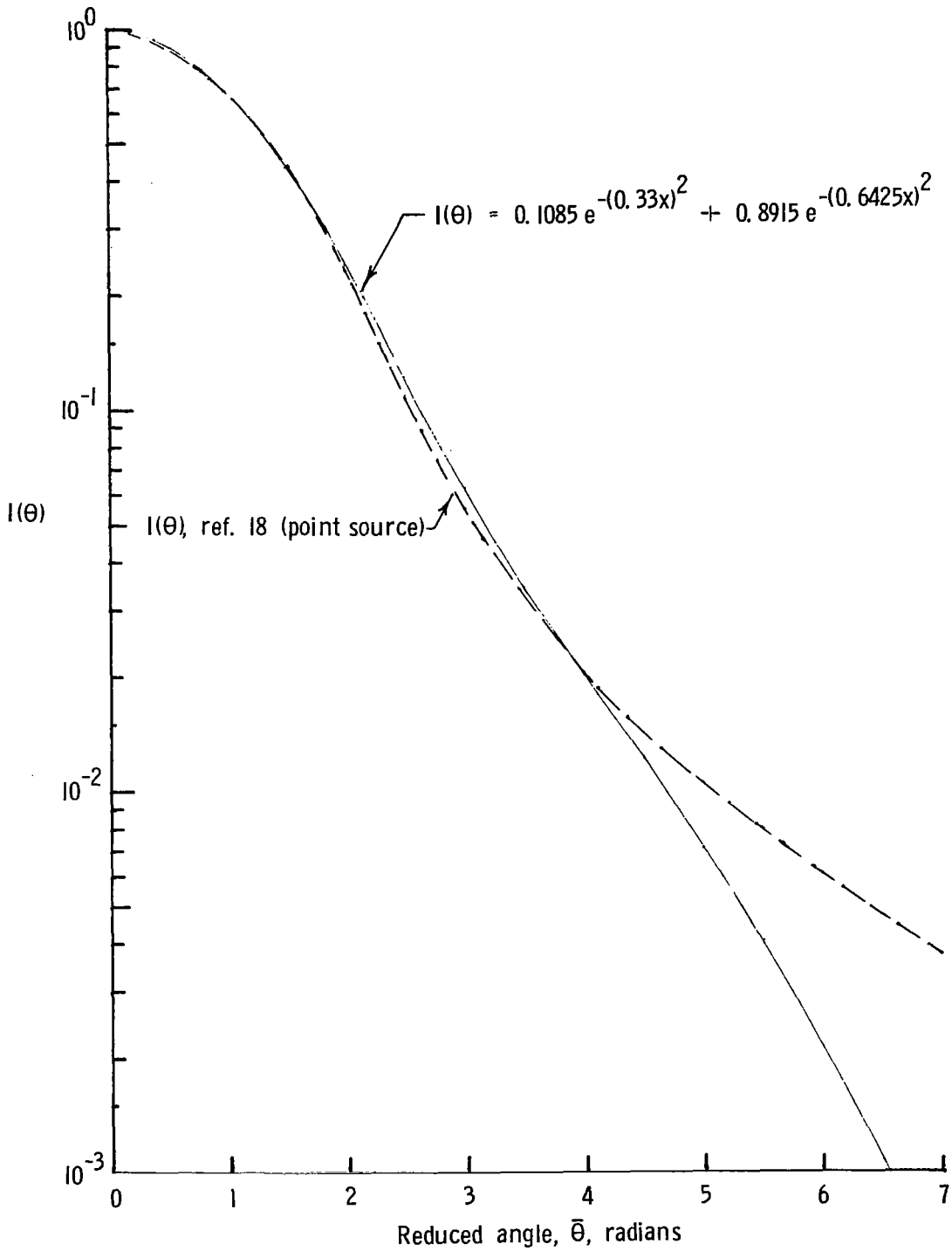

Figure 24.- Comparison of the series approximation of $I(\theta)$ with the original data from reference 18.

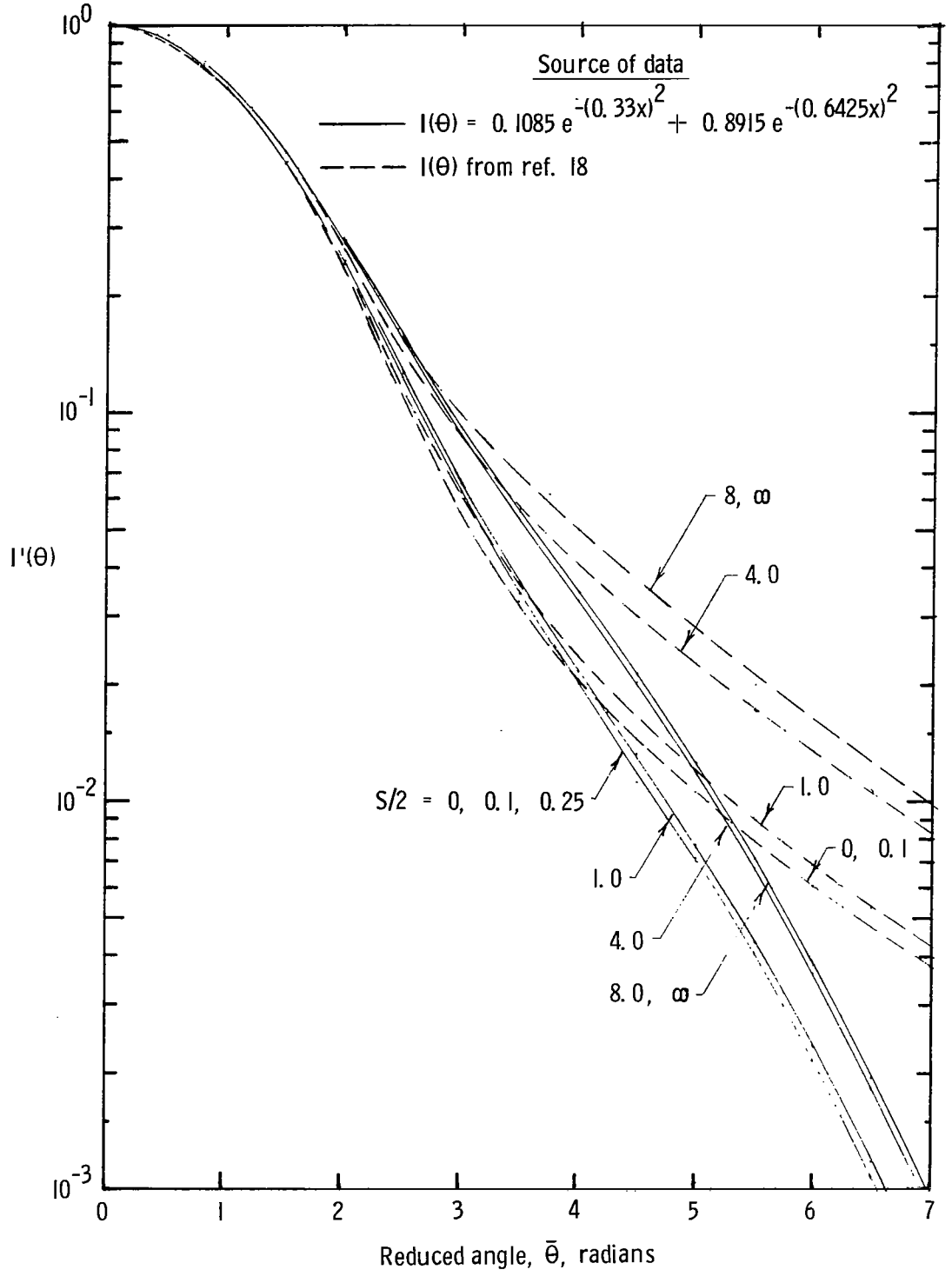

Figure 25.- Normalized intensity as a function of angle for various slit lengths.

REFERENCES

1. Akey, Norman D.: Overview of RAM Reentry Measurements Program. The Entry Plasma Sheath and Its Effects on Space Vehicle Electromagnetic Systems, Vol. 1, NASA SP-252, 1971, pp. 19-31.

2. Cuddihy, William F.; Beckwith, Ivan E.; and Schroeder, Lyle C. (With appendix A by Ivan E. Beckwith, Dennis M. Bushnell, and James L. Hunt; appendix B by Ivan E. Beckwith and Sadie P. Livingston; and appendix C by Ivan E. Beckwith): Flight Test and Analysis of a Method for Reducing Radio Attenuation During Hypersonic Flight. NASA TM X-1331, 1967.

3. Akey, Norman D.; and Cross, Aubrey E. (With appendix A by Thomas G. Campbell; appendix B by Fred B. Beck; and appendix C by W. Linwood Jones, Jr.): Radio Blackout Alleviation and Plasma Diagnostic Results From a 25 000 Foot Per Second Blunt-Body Reentry. NASA TN D-5615, 1970.

4. Bushnell, Dennis M.; and Gooderum, Paul B.: Atomization of Superheated Water Jets at Low Ambient Pressures. J. Spacecraft & Rockets, vol. 5, no. 2, Feb. 1968, pp. 231-232.

5. Priem, Richard J.: Breakup of Water Drops and Sprays With a Shock Wave. Jet Propulsion, vol. 27, no. 10, Oct. 1957, pp. 1084-1087, 1093.

6. Morrell, Gerald: Critical Conditions for Drop and Jet Shattering. NASA TN D-677, 1961.

7. Gooderum, Paul B.; and Bushnell, Dennis M.: Measurement of Mean Drop Sizes for Sprays From Superheated Waterjets. J. Spacecraft & Rockets, vol. 6, no. 2, Feb. 1969, pp. 197-198.

8. Gooderum, Paul B.; and Bushnell, Dennis M.: Incipient Cross-Stream Liquid Jet Atomization at High Altitude and Velocity. J. Spacecraft & Rockets, vol. 7, no. 8, Aug. 1970, pp. 1014-1017.

9. Miesse, C. C.: Advancing Frontiers of Spray Technology. Applied Mechanics Surveys, Spartan Books, Inc., c.1966, pp. 925-930.

10. Forsnes, Victor G.; and Ulrich, Richard D.: A Literature Review and Discussion of Liquid Particle Breakup in Gas Streams. NWC TP 4589, U.S. Navy, July 1968. (Available from DDC as AD 844 075.)

11. Luna, R. E.; and Klikoff, W. A.: On Aerodynamic Breakup of Liquid Drops. SC-RR-66-2716, Sandia Corp., June 1967.

12. Ingebo, Robert D.; and Foster, Hampton H.: Drop-Size Distribution for Crosscurrent Breakup of Liquid Jets in Airstreams. NASA TN 4087, 1957.

13. Volynskiy, M. S.: Atomization of a Liquid in a Supersonic Flow. FTD-MT-63-186, U.S. Air Force, Dec. 6, 1963. (Available from DDC as AD 602 597.)

14. Bitron, Moshe D.: Atomization of Liquids by Supersonic Air Jets. Ind. & Eng. Chem., vol. 47, no. 1, 1955, pp. 23-28.

15. Sherman, Allan; and Schetz, Joseph: Breakup of Liquid Sheets and Jets in a Supersonic Gas Stream. AIAA J., vol. 9, no. 4, Apr. 1971, pp. 666-673.

16. Kurzius, Shelby C.; and Raab, Fredrik H.: Measurement of Droplet Sizes in Liquid Jets Atomized in Low-Density Supersonic Streams. NASA CR-1242, 1968.

17. Gooderum, Paul; Bushnell, Dennis; and Huffman, Jarrett: Mean Droplet Size for Cross-Stream Water Injection Into a Mach 8 Air Flow. J. Spacecraft & Rockets, vol. 4, no. 4, Apr. 1967, pp. 534-536.

18. Dobbins, R. A.; Crocco, L.; and Glassman, I.: Measurement of Mean Particle Sizes of Sprays From Diffractively Scattered Light. AIAA J., vol. 1, no. 8, Aug. 1963, pp. 1882-1886.

19. Roberts, J. H.; and Webb, M. J.: Measurement of Droplet Size for Wide Range Particle Distributions. AIAA J., vol. 2, no. 3, Mar. 1964, pp. 583-585.

20. Brown, Ralph: Sprays Formed by Flashing Liquid Jets. Ph. D. Diss., Univ. of Michigan, 1960.

21. Adelberg, M.: Breakup Rate and Penetration of a Liquid Jet in a Gas Stream. AIAA J., vol. 5, no. 8, Aug. 1967, pp. 1408-1415.

22. Adelberg, M.: Mean Drop Size Resulting From the Injection of a Liquid Jet Into a High-Speed Gas Stream. AIAA J., vol. 6, no. 6, June 1968, pp. 1143-1147.

23. Catton, I.; Hill, D. E.; and McRae, R. P.: Study of Liquid Jet Penetration in a Hypersonic Stream. AIAA J., vol. 6, no. 11, Nov. 1968, pp. 2084-2089.

24. Kolpin, M. A.; Horn, K. P.; and Reichenbach, R. E.: Study of Penetration of a Liquid Injectant Into a Supersonic Flow. AIAA J., vol. 6, no. 5, May 1968, pp. 853-858.

25. Reichenbach, R. E.; and Horn, K. P.: Investigation of Injectant Properties on Jet Penetration in a Supersonic Stream. AIAA J., vol. 9, no. 3, Mar. 1971, pp. 469-472.

26. Hinson, William F.; Gooderum, Paul B.; and Bushnell, Dennis M.: Experimental Investigation of Multiple-Jet Liquid Injection Into Hypersonic Flow. NASA TN D-5861, 1970.

27. Weaver, William L.; and Hinson, William F.: Water Injection From a 9° Hemisphere-Cone Into a Hypersonic Aistream. NASA TN D-5739, 1970.

28. Horn, K. P.; and Reichenbach, R. E.: Further Experiments on Spreading of Liquids Injected Into a Supersonic Flow. AIAA J., vol. 7, no. 2, Feb. 1969, pp. 358-359.

29. Szpiro, Edward J.: Secondary Fluid Injection Into a Supersonic Airstream. Rep. No. 65-2, Mech. Eng. Res. Labs., McGill Univ., Apr. 1965.

30. Schroeder, Lyle C.: Flight Measurements at 25 000 Feet Per Second of Blackout Alleviation by Water and Electrophilic Injection. The Entry Plasma Sheath and Its Effects on Space Vehicle Electromagnetic Systems, Vol. II, NASA SP-253, 1971, pp. 77-100.

31. Schexnayder, Charles J., Jr.; Huber, Paul W.; and Evans, John S.: Calculation of Electron Concentration for a Blunt Body at Orbital Speeds and Comparison With Experimental Data. NASA TN D-6294, 1971.

NASA-Langley, 1972 —— 12 L-8004